



Research papers

A new kinematic wave model that describes lateral subsurface flow and percolation in hillslopes

Yoshito Sugawara^{*}, Takahiro Sayama

Disaster Prevention Research Institute, Kyoto University, Gokasho, Uji, Kyoto 611-0011, Japan

ARTICLE INFO

This manuscript was handled by Corrado Corradini, Editor-in-Chief, with the assistance of Xuan Yu, Associate Editor

Keywords:

Hillslope runoff
Subsurface flow
Kinematic wave model
Percolation
Analytical expression

ABSTRACT

Kinematic wave (KW) models are commonly used for flood forecasting in large river basins, but have limitations in their ability to simulate percolation effects. Here, we suggest an extended KW model wherein the vertical pressure head is under non-hydrostatic conditions. The proposed model uses the Brooks Corey and Mualem models to estimate the water retention curve and unsaturated hydraulic conductivity and adopts the pressure head gradient as a new variable to calculate runoff based on changing water content distributions over time due to percolation. The increase in the pressure head gradient with rainfall infiltration is determined from the relationship between water storage and pressure head distribution, while the decrease in pressure head gradient due to percolation is modeled as exponential decay with time. A comparison of the proposed KW model and a numerical solution of the Richards equation shows that the proposed KW model can reproduce the storage effect caused by percolation, delaying runoff and reducing peak discharge. The agreement between the proposed KW model and the Richards equation is high for soils with high water retention. Conversely, the agreement becomes lower for soil with low water retention or deep soil layer thickness, where the complexity of water content distribution requires further refinement. The proposed model can easily be incorporated into distributed models while low computational cost with keeping the important percolation effects.

1. Introduction

Subsurface flow is a crucial component of mountainous rainfall-runoff processes (Dunne and Black, 1970; Freeze, 1972), but hydrological models that simulate unsaturated and saturated flow in hillslopes with three-dimensional discretization (Kampf and Burges, 2007) can be computationally expensive for large river basins. Flood forecasting systems adopt distributed models that use lower dimensional lateral flow models, which are suitable for high spatial resolution in large areas because of their computational cost, to address this issue. However, these models typically lump vertical water distributions and treat unsaturated and saturated zones together (Du et al., 2007; Sayama et al., 2012; Tanaka and Tachikawa, 2015), requiring creative solutions for physical calculations. Some widely used models, such as ParFlow (Kollet and Maxwell, 2006) and CATHY (Paniconi et al., 2003), solve the three-dimensional Richards equation, while others, including GSSHA (Downer and Ogden, 2004) and SHE (Abbott et al., 1986), solve the vertical unsaturated flow and two-dimensional lateral flow separately. Despite the advantages of these models in describing unsaturated and saturated flow

in detail, their computational cost can be prohibitive for large-scale flood forecasting systems such as the one for the whole of Europe (Thielen et al., 2009) and significant numbers of the medium-to-small river basins (Alfieri et al., 2012; Sayama et al., 2020) that require high resolution and long lead times.

Many large-scale simulation models employ a lateral flow model based on the Boussinesq equation, which describes saturated lateral flow over an impermeable bedrock (Childs, 1971). The equation combines Darcy's law and the Dupuit-Forchheimer assumption, which presumes that flow lines are parallel to the bedrock. In steep hillslopes, the kinematic wave (KW) models are often used to account for the gravity flow in the Boussinesq equation (Beven, 1981; Takasao and Shiiba, 1988). Fan and Bras (1998) proposed a KW model that accounts for variations in slope width and soil thickness as functions of the downstream distance.

Extensions of the Boussinesq equation are widely suggested in the literature. Troch et al. (2003) developed the hillslope-storage Boussinesq (HSB) model to analyze runoff characteristics for a basic set of characteristic hillslope shapes. Hilberts et al. (2005) derived the drainable porosity, which changes depending on water depth, in an analytical

^{*} Corresponding author.

E-mail address: sugawara.yoshito.2h@kyoto-u.ac.jp (Y. Sugawara).

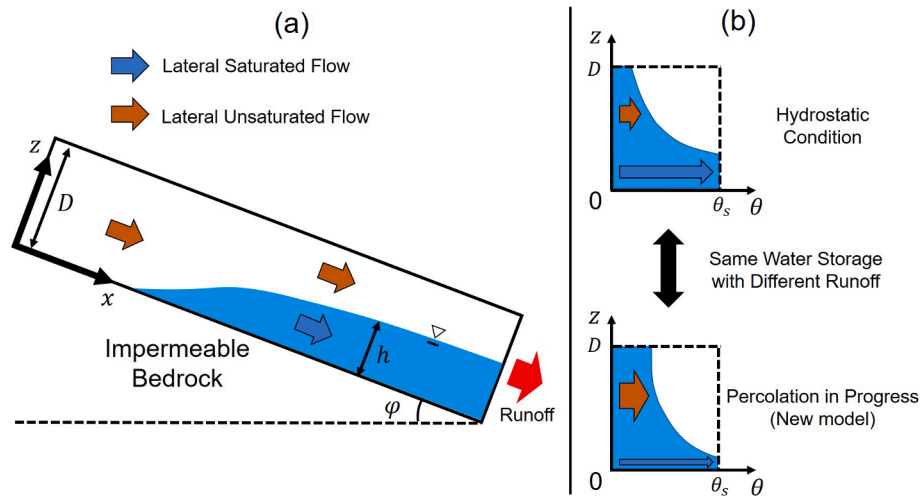


Fig. 1. (a) Schematic diagram of the slope structure and runoff process in this study. (b) A water distribution along z direction. When the percolation along z direction is in progress, the lateral runoff is smaller than it in the hydrostatic condition.

form based on soil physical parameters and applied it to the HSB model. Hilberts et al. (2007) proposed a model that couples the HSB model with the one-dimensional Richards equation to reflect vertical flow in the unsaturated zone. The Boussinesq equation ignores the effect of unsaturated zones and requires improvement for a more realistic analysis.

Hillslope flow is often unsaturated; therefore, various authors have sought to include the effects of unsaturated flow. Ciarapica and Todini (2002) modeled unsaturated lateral flow as a function of mean volumetric water content, while Kubota and Sivapalan (1995) assumed a more general condition with the saturated hydraulic conductivity decreasing depending on the soil depth. Tachikawa et al. (2004) proposed a KW model that integrally solves lateral unsaturated and saturated flow. They assumed that the soil layer comprises a large pore dominated by lateral saturated subsurface flow and a matrix pore dominated by unsaturated flow. This model reflects the transition from unsaturated to saturated flow when rainfall first enters the matrix pore and fills the large pore after the matrix pore becomes saturated (Sayama and McDonnell, 2009). Several studies investigated and improved the applicability of the KW model; examples include comparing it to a numerical solution of the Richards equation under various conditions (An et al., 2010), reflecting the pressure term of Darcy's law (Hunukumbura et al., 2012) and investigating how to determine parameters reproducing runoff from the soil layer containing a pipe (Ichikawa et al., 2021). These modifications add a degree of freedom to models and have generally been shown to improve model fit; however, several aspects are left unaddressed in these models.

Lateral flow models that do not consider water distributions in the unsaturated zone have difficulty in determining the threshold when the lateral saturated flow occurs, but recent studies have attempted to fill this gap. The models proposed by Pan et al. (2015), Kong et al. (2016), and Sugawara and Sayama (2021) directly use parameters from the water retention curve to model lateral unsaturated and saturated flow, assuming a hydrostatic condition along the direction perpendicular to bedrock and integrating the distribution of hydraulic conductivity. This allows for a calculation of runoff by lumping the perpendicular distribution. Sugawara and Sayama (2021) adopted the Brooks-Corey and Mualem models (Brooks and Corey, 1966; Mualem, 1976) for the water retention curve and unsaturated hydraulic conductivity to derive the analytical relationship between the water storage in the soil layer and runoff. In this model, the threshold at which the lateral saturated flow occurs is determined from the water retention curve, soil thickness, and slope gradient. However, these models do not consider the effects of percolation, which is crucial for rainfall-runoff transformation (Tani et al., 2020).

Here, we develop a KW model that considers percolation. In particular, we extend the current assumption of hydrostatic distribution to a dynamic linear distribution. The relationship between the water storage and runoff in the hillslope is formulated by integrating distributions of the water content and hydraulic conductivity obtained from the pressure head. We compare the proposed KW model with a numerical solution of the Richards equation to evaluate the model's performance.

2. Methods

2.1. Fundamental equations

Fig. 1a shows a schematic diagram of the slope structure and runoff process in this study. It assumes a steep hillslope with highly permeable soil, where all rainfall infiltrates the soil layer without Hortonian overland flow. For simplicity, the slope width is assumed to be the unit length. The continuity equation is

$$\frac{\partial S}{\partial t} + \frac{\partial q}{\partial x} = r \cos \varphi \quad (1)$$

where S [L] is the water storage in a unit slope length, q [L^2T^{-1}] is the lateral discharge, t [T] is time, x [L] is the downward coordinate along the bedrock, r [LT^{-1}] is rainfall intensity, and φ [-] is the slope angle. Since this study considers both unsaturated and saturated zones, the storage S is defined as

$$S = \int_0^D \theta dz \quad (2)$$

where z [L] is the perpendicular upward coordinate with respect to the bedrock, θ [-] is the volumetric water content, and D [L] is the thickness of the soil layer. Darcy's law along the x direction is

$$v_x = K \sin \varphi - K \frac{\partial \psi}{\partial x} \quad (3)$$

where v_x [LT^{-1}] is the Darcy velocity along the x direction, K [LT^{-1}] is the unsaturated hydraulic conductivity, and ψ [L] is the pressure head. We adopt the KW model, which considers only gravity-driven flow ($\frac{\partial \psi}{\partial x} = 0$) (e.g., Beven, 1981; Takasao and Shiiba, 1988; Fan and Bras, 1998):

$$v_x = K \sin \varphi \quad (4)$$

The lateral discharge is obtained by integrating equation (4):

$$q = \int_0^D v_z dz = \sin\varphi \int_0^D K dz \quad (5)$$

The runoff from the hillslope can be calculated by coupling equation (1) and the relationship between S and q can be determined from equations (2) and (5). Sugawara and Sayama (2021) derived the analytical relationship between S and q based on the Brooks-Corey and Mualem models by assuming the hydrostatic condition along the z direction. The hydrostatic condition here implies that the percolation process along the z direction is ignored, and rainwater infiltrating the soil layer is immediately stored on the bedrock. Darcy's law along the z direction is expressed as

$$v_z = -K \cos\varphi - K \frac{\partial\psi}{\partial z} \quad (6)$$

where v_z [LT^{-1}] is the Darcy velocity along the z direction. Assuming the hydrostatic condition ($v_z = 0$), we obtain the following equation:

$$\frac{\partial\psi}{\partial z} = -\cos\varphi \quad (7)$$

This yields the pressure head distribution along the z direction, and the distributions of unsaturated hydraulic conductivity and water content are determined. By incorporating these distributions into equations (2) and (5), we can obtain the analytical relationship between S and q . Similarly, Pan et al. (2015) derived a low-dimensional lateral flow model from the three-dimensional Richards equation by integrating the perpendicular hydrostatic distribution. Kong et al. (2016) also improved the HSB model (Troch et al., 2003) by considering lateral unsaturated flow by assuming the perpendicular hydrostatic condition to the bedrock. Although these models consider the perpendicular water content distribution, they do not account for the percolation process from the soil surface to the bedrock owing to their assumption of the hydrostatic condition. As shown in Fig. 1b, the hydrostatic condition results in a high water content area on the bedrock, leading to a large lateral discharge. By contrast, incomplete percolation leads to lesser discharge, even with the same storage. To incorporate the percolation process into lateral flow models, they are combined with the one-dimensional Richards equation, as described by Hilberts et al. (2007). However, this requires discretization along the perpendicular direction, which increases the computational cost.

2.2. Derivation of a new KW model

We propose a new method to reflect percolation effects in a KW model without perpendicular discretization. The pressure head, which was assumed to be in hydrostatic condition, is extended to the non-hydrostatic condition:

$$\frac{\partial\psi}{\partial z} = a \quad (8)$$

where a [-] is the pressure head gradient that is allowed to vary in time. When $a = 0$, a pressure head distribution is uniform across the entire soil layer. For $a > 0$, the pressure head is highest at the soil surface and decreases with depth, while for $a < 0$, the opposite occurs. The value of a increases when the near-surface area becomes wet due to rainfall. Thereafter, the value of a decreases along with percolation and converges to the hydrostatic condition ($a = -\cos\varphi$). Although the actual distributions of pressure head during a rainfall event are complex, the main focus of this study is to model the effect of the dynamically changing perpendicular water distribution on the lateral flow. From equation (8), the pressure head distribution becomes

$$\psi = az + \psi_b \quad (9)$$

where ψ_b [L] is the pressure head at the bottom of the soil layer. The

Brooks-Corey and Mualem models (Brooks and Corey, 1966; Mualem, 1976) are used for the water retention curve and unsaturated hydraulic conductivity to solve equations (2) and (5):

$$S_e = \frac{\theta - \theta_r}{\theta_s - \theta_r} = \begin{cases} \left(\frac{\psi_e}{\psi}\right)^\lambda (\psi \leq \psi_e) \\ 1 (\psi > \psi_e) \end{cases} \quad (10)$$

$$K = k_s \bullet k_r = k_s \bullet S_e^n \quad (11)$$

where S_e [-] is the effective saturation rate, k_r [-] is the relative hydraulic conductivity, θ_s [-] is the saturated volumetric water content, θ_r [-] is the residual volumetric water content, ψ_e [L] is the air entry pressure head, k_s [LT^{-1}] is saturated hydraulic conductivity, λ [-] is the pore size distribution, and n [-] is defined as $n = 2 + l + 2/\lambda$, with l [-] as the pore tortuosity-connectivity coefficient ($l = 0.5$ in this study). The case of the uniform pressure head distribution ($a = 0$) is self-explanatory and will be omitted. To ensure that the model is physically reasonable, we make the following assumptions in this study.

- $aD + \psi_b \leq \psi_e$. $aD + \psi_b$ is the pressure head at the soil surface. Hence, the Hortonian overland flow is not considered since the pressure head at the soil surface does not exceed the condition with full saturation of the soil layer.
- $-\cos\varphi \leq a \leq \cos\varphi$. $a < -\cos\varphi$ may occur where groundwater exfiltrates from the bedrock, but the bedrock is assumed to be effectively impermeable in this study. In addition, $a > \cos\varphi$ is a case of extreme wetness near the soil surface and is not considered in this study because we assume the soil permeability well exceeds the rainfall rate.
- $S > \theta_r D$. This constraint means that only the flow within the effective porosity ($\theta_s - \theta_r$) is considered.

To determine the threshold of S at which the saturated zone on the bedrock occurs, we assign $\psi_b = \psi_e$ in equation (9) and substitute it in equation (10):

$$\theta = \theta_r + (\theta_s - \theta_r) \left(\frac{\psi_e}{az + \psi_e} \right)^\lambda \quad (12)$$

Substituting equation (12) in equation (2), we obtain the threshold value S_{thre} [L]:

$$S_{thre}(a) = \theta_r D + \frac{\psi_e (\theta_s - \theta_r)}{a(1 - \lambda)} \left[\left(\frac{aD + \psi_e}{\psi_e} \right)^{1-\lambda} - 1 \right] \quad (13)$$

This S_{thre} is used to classify lateral flow patterns. When $\theta_r D < S < S_{thre}$, only lateral unsaturated flow occurs. When $S_{thre} \leq S \leq \theta_s D$, lateral unsaturated and saturated flows occur simultaneously. In a previous study where $a = -\cos\varphi$ was always assumed (Sugawara and Sayama, 2021), S_{thre} was constant. However, in the present study, S_{thre} is more realistic because the occurrence of the saturated zone is affected by percolation.

We will derive the relationship between S and q . The saturated water depth h is defined by the range of z that satisfies $\psi \geq \psi_e$ from equation (9):

$$h = \begin{cases} 0 (\theta_r D < S < S_{thre}) \\ \frac{\psi_e - \psi_b}{a} (S_{thre} \leq S \leq \theta_s D) \end{cases} \quad (14)$$

The distributions of θ and K are obtained from equations (9), (10), and (11):

$$\theta = \begin{cases} \theta_r + (\theta_s - \theta_r) \left(\frac{\psi_e}{az + \psi_b} \right)^\lambda (h \leq z \leq D) \\ \theta_s (0 < z < h) \end{cases} \quad (15)$$

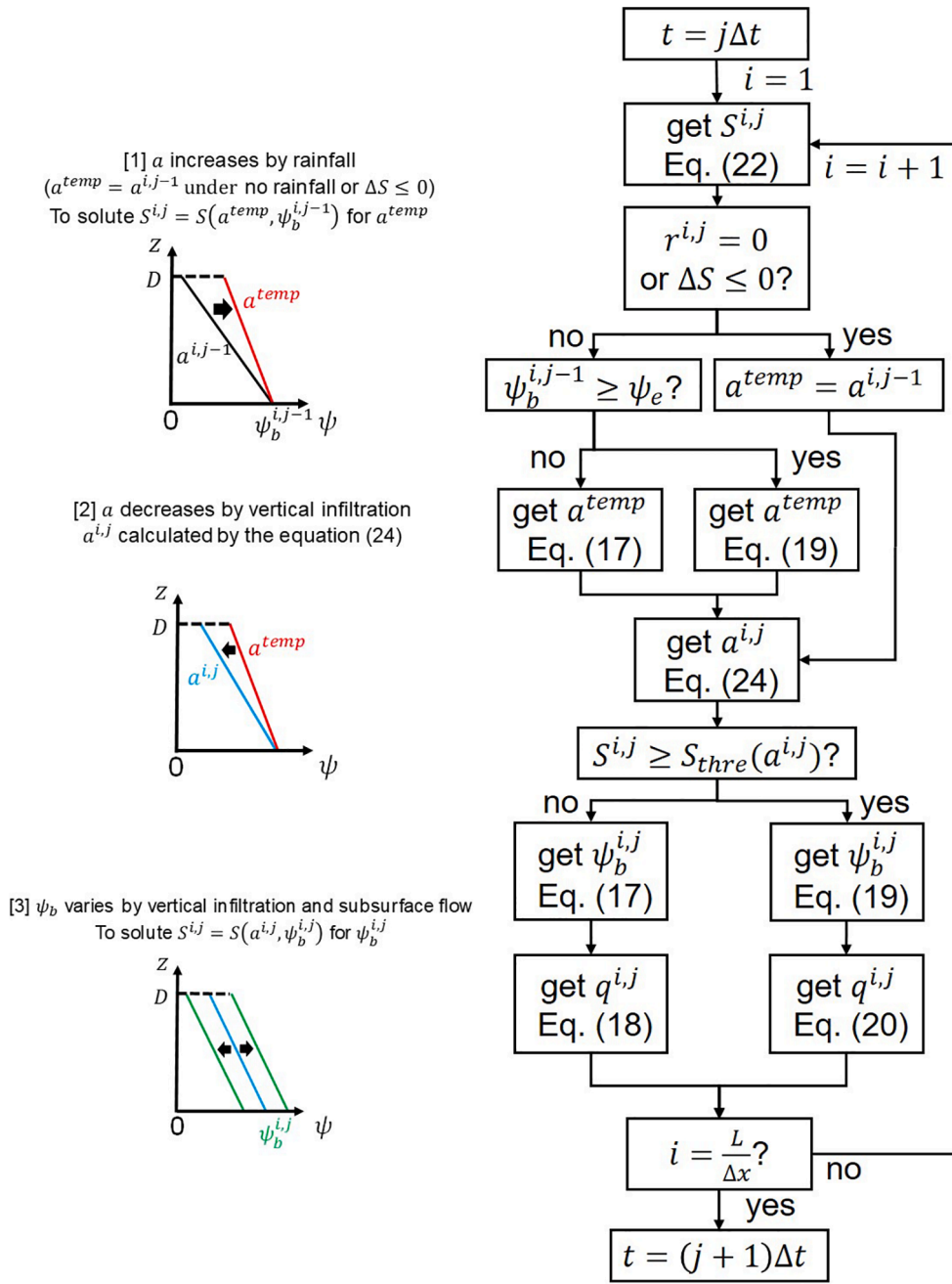


Fig. 2. Process to estimate pressure head gradient a and bottom pressure head ψ_b and a flowchart for using the proposed analytical equations.

$$K = \begin{cases} k_s \left(\frac{\psi_e}{az + \psi_b} \right)^{n\lambda} & (h \leq z \leq D) \\ k_s & (0 < z < h) \end{cases} \quad (16)$$

Substituting equation (15) in equation (2) and equation (16) in equation (5), and then classifying the case based on equation (14), the following relationships are obtained:

Before establishing a saturated zone on the bedrock (i.e., $\theta_r D < S < S_{thre}$)

$$S(a, \psi_b) = \theta_r D + \frac{\psi_e(\theta_s - \theta_r)}{a(1 - \lambda)} \left[\left(\frac{aD + \psi_b}{\psi_e} \right)^{1-\lambda} - \left(\frac{\psi_b}{\psi_e} \right)^{1-\lambda} \right] \quad (17)$$

$$q(a, \psi_b) = \frac{k_s \psi_e \sin \varphi}{a(1 - n\lambda)} \left[\left(\frac{aD + \psi_b}{\psi_e} \right)^{1-n\lambda} - \left(\frac{\psi_b}{\psi_e} \right)^{1-n\lambda} \right] \quad (18)$$

For conditions with a saturated zone (i.e., $S_{thre} \leq S \leq \theta_s D$)

$$S(a, \psi_b) = \theta_s \frac{\psi_e - \psi_b}{a} + \theta_r \left(D - \frac{\psi_e - \psi_b}{a} \right) + \frac{\psi_e(\theta_s - \theta_r)}{a(1 - \lambda)} \left[\left(\frac{aD + \psi_b}{\psi_e} \right)^{1-\lambda} - 1 \right] \quad (19)$$

$$q(a, \psi_b) = k_s \frac{\psi_e - \psi_b}{a} \sin \varphi + \frac{k_s \psi_e \sin \varphi}{a(1 - n\lambda)} \left[\left(\frac{aD + \psi_b}{\psi_e} \right)^{1-n\lambda} - 1 \right] \quad (20)$$

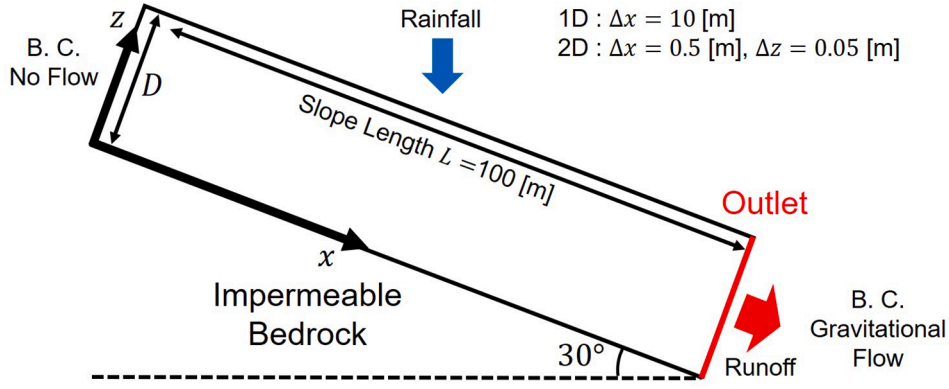


Fig. 3. Schematic diagram of the simulation domain.

2.3. Estimation method and calculation procedure for

The relationship between S and q expressed by equations (17), (18), (19), and (20) has two auxiliary variables: a and ψ_b . If $a = -\cos\varphi$, the runoff in the hillslope is calculated from the continuity equation and the relationship between S and q . However, these equations cannot be easily solved owing to the increase in the number of variables. Estimating the progress of percolation separately from the continuity equation is necessary. Therefore, an exponential decay model is introduced in this study to estimate a :

$$\frac{da}{dt} = \frac{-a + \cos\varphi}{\tau} \quad (21)$$

where τ [T] is the relaxation time. τ is inherently dependent on water content but is considered a constant in this study for simplicity. The time variation of a is the largest at $a = \cos\varphi$ and becomes smaller as a approaches the hydrostatic condition. The exponential decay model is occasionally used as a simple way to calculate soil water content (e.g., Arnold et al., 1998; Ross and Smettem, 2000). The specific calculation procedure is shown below. The explicit-based discretization of equation (1) is as follows:

$$\frac{S^{i,j} - S^{i,j-1}}{\Delta t} + \frac{q^{i,j-1} - q^{i-1,j-1}}{\Delta x} = r^{i,j} \cos\varphi \quad (22)$$

where i is the spatial step and j is the time step. If L is the slope length, $i = 1, 2, \dots, \frac{L}{\Delta x}$. When variables $S^{i,j-1}$, $q^{i,j-1}$, $a^{i,j-1}$, and $\psi_b^{i,j-1}$ in the time step $j-1$ are known, we show the procedures to estimate unknown variables $S^{i,j}$, $q^{i,j}$, $a^{i,j}$, and $\psi_b^{i,j}$ in the time step j (Fig. 2). In the beginning, $S^{i,j}$ is obtained by computing equation (22). Next, we follow the three procedures shown in Fig. 2. First, the increased pressure head gradient a^{temp} by rainfall is calculated. However, if there is no rainfall ($r^{i,j} = 0$) or if lateral flow predominates ($\Delta S = S^{i,j} - S^{i,j-1} \leq 0$), we regard $a^{temp} = a^{i,j-1}$. Assuming no effect of rainfall on ψ_b , $S^{i,j} = S(a^{temp}, \psi_b^{i,j-1})$ is solved for a^{temp} (equation (17) is used in the case of $\psi_b^{i,j-1} < \psi_e$ and equation (19) in the case of $\psi_b^{i,j-1} \geq \psi_e$). Second, $a^{i,j}$ decreasing by the progress of percolation is calculated. The decrease of a during the time Δt is obtained by integrating equation (21).

$$\int_{a^{temp}}^{a^{i,j}} \frac{da}{a + \cos\varphi} = -\frac{1}{\tau} \int_0^{\Delta t} dt \quad (23)$$

The solution of equation (23) is

$$a^{i,j} = -\cos\varphi + (a^{temp} + \cos\varphi) \exp\left(-\frac{\Delta t}{\tau}\right) \quad (24)$$

Using equation (24), the next time step $a^{i,j}$ varied by rainfall and

percolation can be obtained. Third, the next time step $\psi_b^{i,j}$, which is varied by percolation and lateral flow, is calculated. Because $S^{i,j}$ and $a^{i,j}$ are known, $\psi_b^{i,j}$ is determined by solving $S^{i,j} = S(a^{i,j}, \psi_b^{i,j})$ (equation (17) is used in the case of $S^{i,j} < S_{thre}(a^{i,j})$ and equation (19) in the case of $S^{i,j} \geq S_{thre}(a^{i,j})$). Finally, we can obtain $q^{i,j}$ from the known $S^{i,j}$, $a^{i,j}$, and $\psi_b^{i,j}$ by using equation (18) or (20).

3. Models and simulation setup for comparison

To evaluate the newly proposed KW model in this study (1D-New), we compare it with the original KW model that assumes the hydrostatic condition $a = -\cos\varphi$ (1D-Hs) and a model numerically to solve the two-dimensional Richards equation (2D-RE).

3.1. The KW model 1D-Hs

The 1D-Hs is the KW model that does not consider the effect of percolation and was developed by Sugawara and Sayama (2021). It is derived by assuming $a = -\cos\varphi$ and using the same procedure as in this study. From equation (13), S_{thre} is given by the following equation:

$$S_{thre} = \theta_r D + \frac{\psi_e(\theta_s - \theta_r)}{\cos\varphi(1-\lambda)} \left[1 - \left(\frac{\psi_e - D\cos\varphi}{\psi_e} \right)^{1-\lambda} \right] \quad (25)$$

S_{thre} in the 1D-Hs is constant, unlike in the 1D-New. From equations (17), (18), (19), and (20), the relationships between S and q can be obtained as follows:

When $\theta_r D < S < S_{thre}$,

$$S(\psi_b) = \theta_r D + \frac{\psi_e(\theta_s - \theta_r)}{\cos\varphi(1-\lambda)} \left[\left(\frac{\psi_b}{\psi_e} \right)^{1-\lambda} - \left(\frac{\psi_b - D\cos\varphi}{\psi_e} \right)^{1-\lambda} \right] \quad (26)$$

$$q(\psi_b) = \frac{k_s \psi_e \sin\varphi}{\cos\varphi(1-n\lambda)} \left[\left(\frac{\psi_b}{\psi_e} \right)^{1-n\lambda} - \left(\frac{\psi_b - D\cos\varphi}{\psi_e} \right)^{1-n\lambda} \right] \quad (27)$$

When $S_{thre} \leq S \leq \theta_s D$,

$$S(\psi_b) = \theta_s \frac{\psi_b - \psi_e}{\cos\varphi} + \theta_r \left(D - \frac{\psi_b - \psi_e}{\cos\varphi} \right) + \frac{\psi_e(\theta_s - \theta_r)}{\cos\varphi(1-\lambda)} \left[1 - \left(\frac{\psi_b - D\cos\varphi}{\psi_e} \right)^{1-\lambda} \right] \quad (28)$$

$$q(\psi_b) = k_s \frac{\psi_b - \psi_e}{\cos\varphi} \sin\varphi + \frac{k_s \psi_e \sin\varphi}{\cos\varphi(1-n\lambda)} \left[1 - \left(\frac{\psi_b - D\cos\varphi}{\psi_e} \right)^{1-n\lambda} \right] \quad (29)$$

In the 1D-Hs model, the only auxiliary variable in the relationship between S and q is ψ_b . Therefore, the runoff calculation can be performed by simply coupling the relationship between S and q with equation (1).

Table 1
The parameters of water retention curve.

Soil Type	θ_s	θ_r	ψ_e [m]	λ
Loam	0.46	0.03	-0.11	0.22
Sand	0.44	0.02	-0.072	0.59
Clay	0.48	0.09	-0.37	0.13
Silt	0.50	0.02	-0.21	0.21

In the 1D-New and 1D-Hs, the surface runoff is modeled by a KW model with the Manning formula when the soil layer is fully saturated.

3.2. The numerical solution of the Richards equation 2D-RE

The 2D-RE is the model numerically to solve the two-dimensional Richards equation, which describes the saturated and unsaturated flow in detail. The two-dimensional Richards equation is expressed as

$$\frac{\partial \theta}{\partial t} = \frac{\partial}{\partial x} K \left(\frac{\partial \psi}{\partial x} - \sin \varphi \right) + \frac{\partial}{\partial z} K \left(\frac{\partial \psi}{\partial z} + \cos \varphi \right) \quad (30)$$

For calculation, we use the program developed by An and Yu (2014) with a minor modification for using the same one as the water retention curve and unsaturated hydraulic conductivity of the 1D-New and 1D-Hs. Equations (10) and (11) are used for the water retention curve and unsaturated hydraulic conductivity. Iterative calculations are conducted in each time steps until the computational error is less than a threshold. Surface runoff is also tracked using the St. Venant equation.

3.3. Slope conditions, parameters and input rainfall data

Fig. 3 shows the schematic diagram of the slope to be analyzed in this study. The computational domain is a rectangular slope with the slope

length $L = 100$ [m] and the angle $\varphi = 30^\circ$. Rainfall infiltrates from the soil surface, and the bedrock is impermeable. The upstream boundary condition is no flow, and the downstream boundary condition is gravity flow by the slope gradient. In the 1D-New and 1D-Hs, the spatial resolution is $\Delta x = 10$ [m], and the temporal resolution is $\Delta t = 300$ [sec]. No discretization is required along the z direction. In the 2D-RE, the spatial resolutions are $\Delta x = 0.5$ [m] and $\Delta z = 0.05$ [m], and the temporal resolutions vary according to the iterative calculations. Table 1 shows the parameters of the water retention curves used in this study, and Fig. 4 shows the soil water retention curves and relative hydraulic conductivity for the parameter sets in Table 1. The soil types and parameters are from the study conducted by Rawls et al. (1982), in which a catalog of soil parameters was estimated from large data sets of soil properties. However, the saturated hydraulic conductivity was separately set because the original saturated hydraulic conductivity may cause Hortonian overland flow in the 2D-RE. Since the proposed method in this study assumes that all rainfall infiltrates into the soil layer, the model performance cannot be properly evaluated if Hortonian overland flow occurs in the 2D-RE. Therefore, in this study, the saturated hydraulic conductivity was set high so that all rainfall infiltrates into the soil layer

Table 2
The parameter sets for the simulation.

No.	Soil Type	k_s [m/sec]	D [m]	τ [sec]	Init. S [m]
1	Loam	0.001	2	7600	0.49
2	Sand	0.001	2	35,000	0.25
3	Clay	0.001	2	2800	0.60
4	Silt	0.001	2	4000	0.52
5	Loam	0.0005	2	15,000	0.49
6	Loam	0.0001	2	76,000	0.49
7	Loam	0.001	3	18,000	0.74

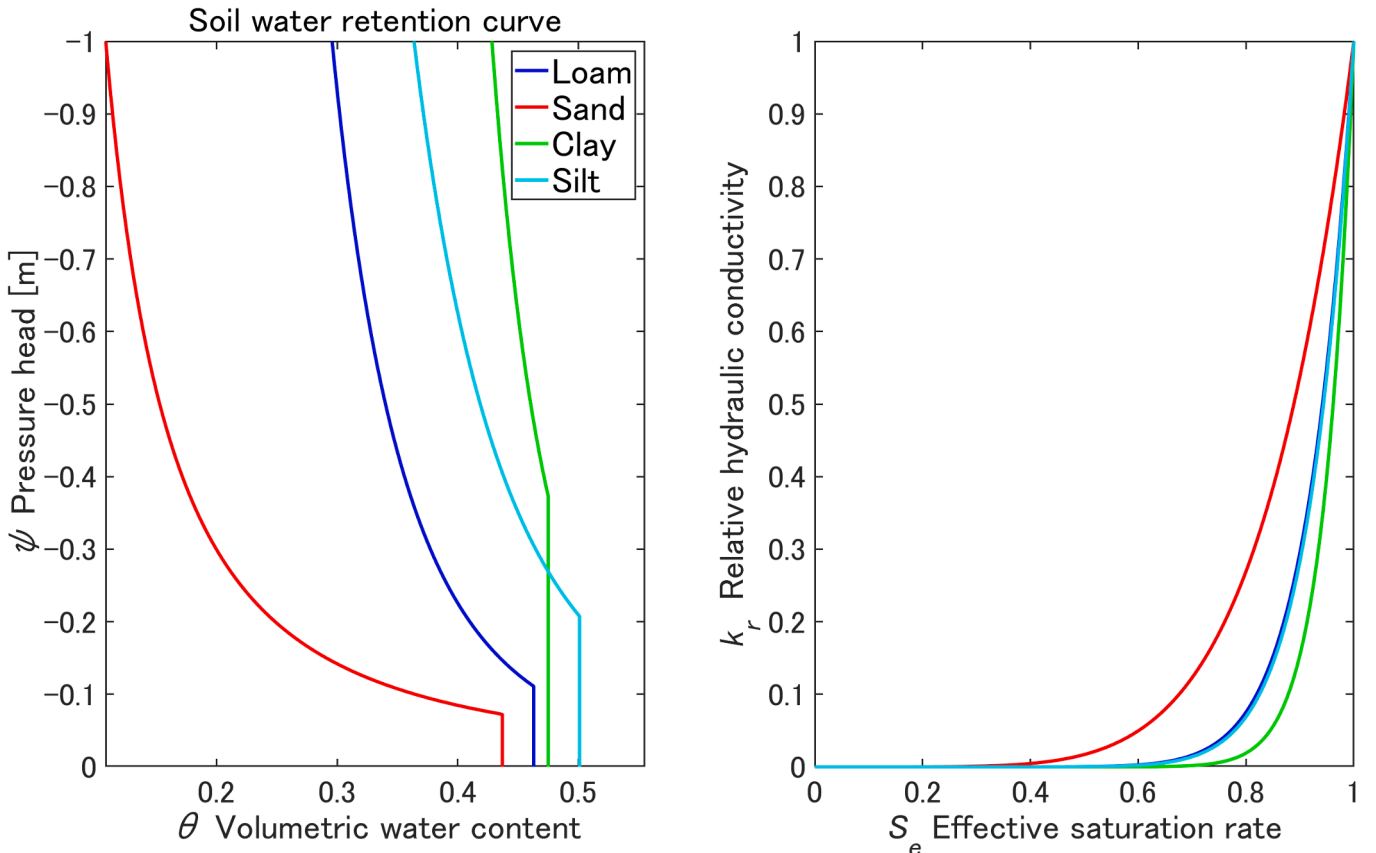


Fig. 4. Soil water retention curves and relative hydraulic conductivity for the parameter sets in Table 1.

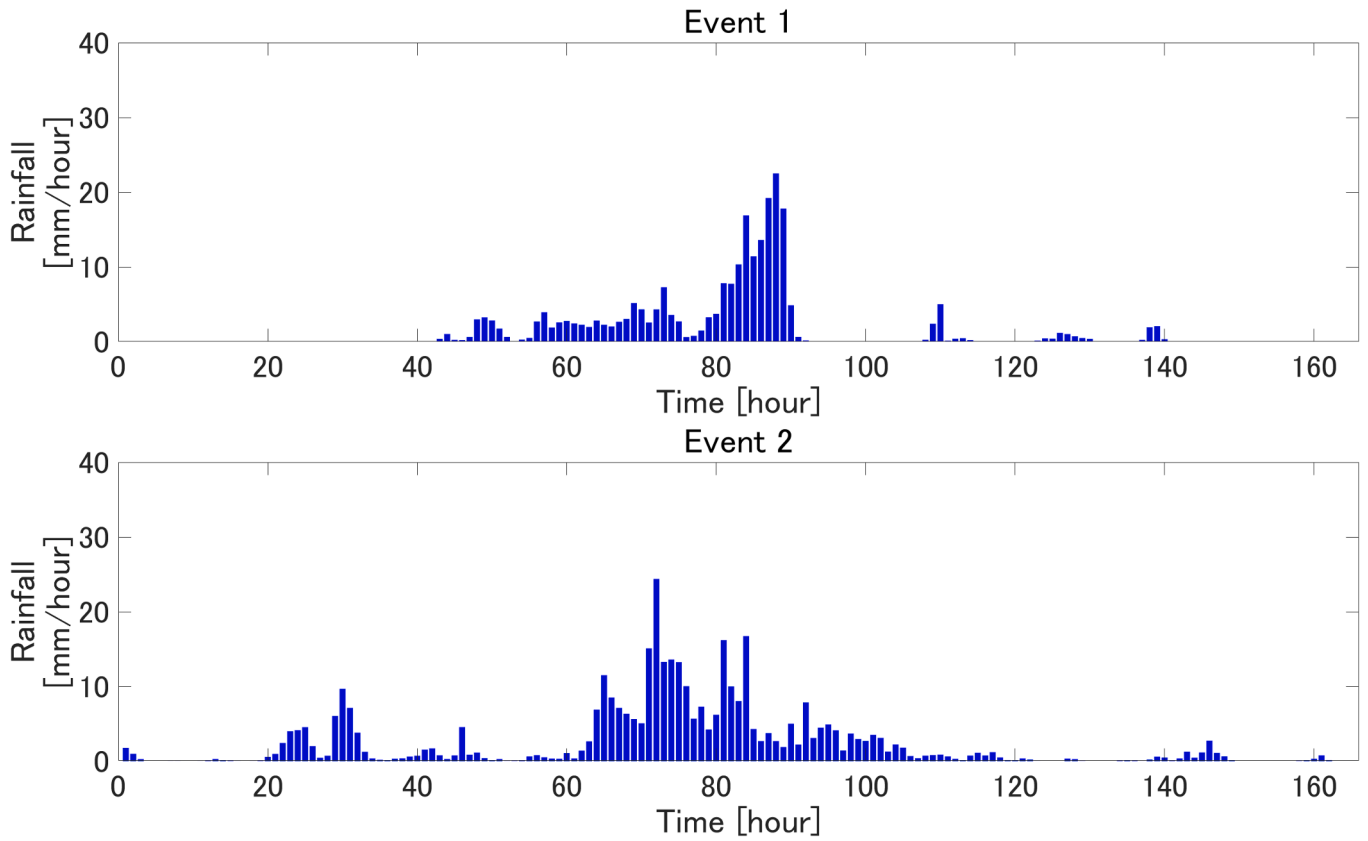


Fig. 5. Input rainfall data for the simulation. The total rainfall is 239 mm in event 1 and 382 mm in event 2.

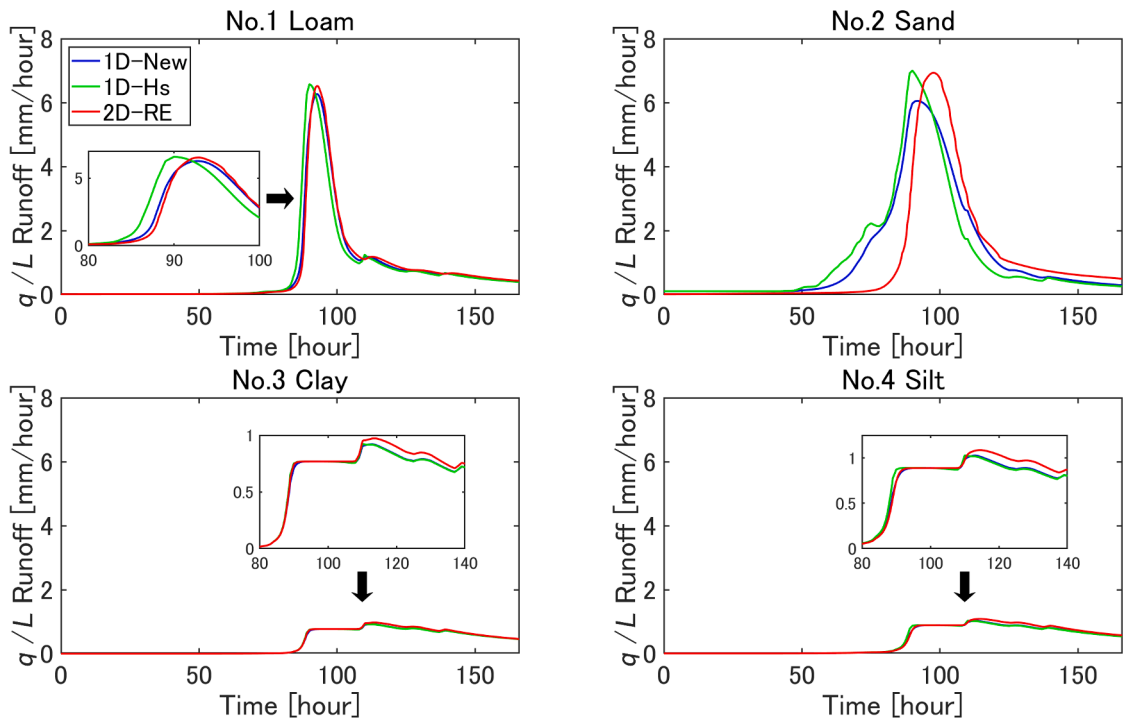


Fig. 6. Hydrographs of event 1 with the parameter sets No. 1–4. The runoff is calculated to divide q at the outlet by slope length L .

even in the 2D-RE. Table 2 shows the parameter sets used in the simulation. We analyzed the effects of changing the water retention curve, saturated hydraulic conductivity, and soil layer thickness. Note that for clay, the saturated hydraulic conductivity is much higher than the

representative values. This is to avoid the occurrence of Hortonian overland flow in the 2D-RE, which is influenced by many conditions (e.g., the water retention curve, rainfall intensity and pattern, slope angle, initial condition, and so on). It is not clear how low the saturated

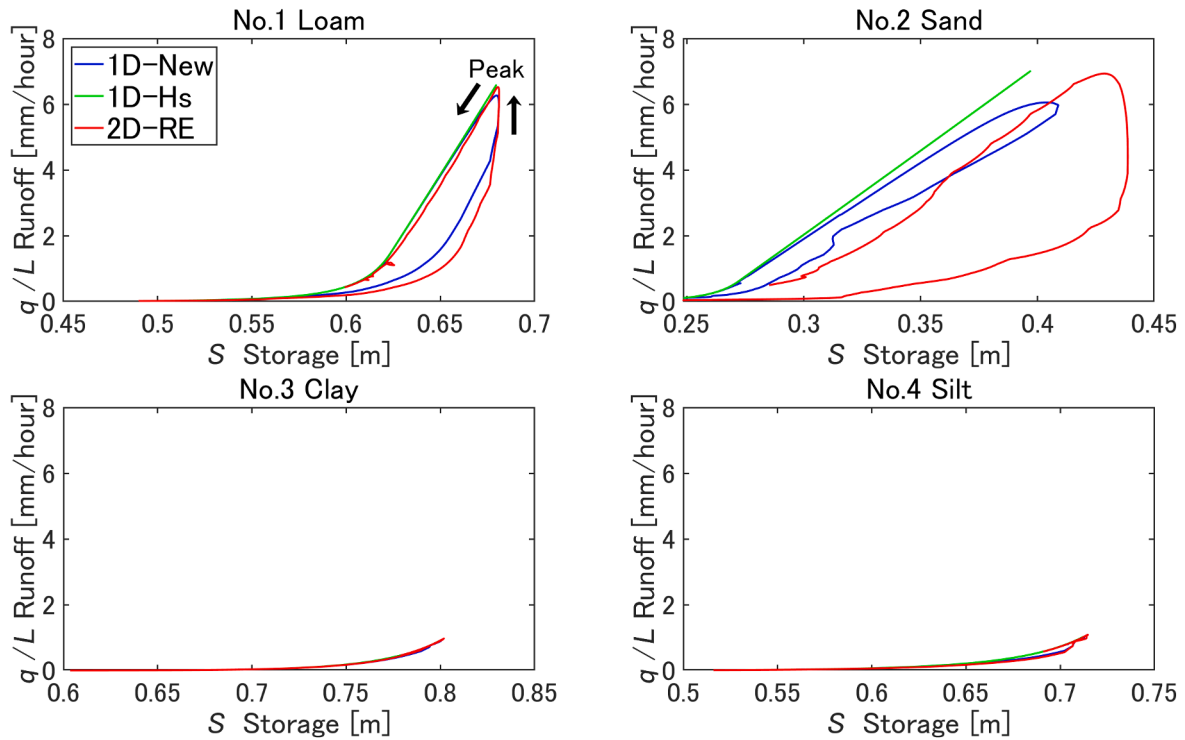


Fig. 7. Storage-runoff relationships of event 1 with the parameter sets No. 1–4. The Storage is S at the outlet, and S of the 2D-RE is calculated by integrating θ along z direction. The path represents changes over time, and the arrows indicate the direction of change. The time of the largest runoff corresponds to the peak time.

hydraulic conductivity can be set for comparison with the proposed method in the two-dimensional simulations. In addition, the previous studies, which used the distributed hydrological models including the kinematic wave model, set the saturated hydraulic conductivity higher than representative value to reproduce observation during storm event (Hunukumbura et al., 2012; Sayama et al., 2012; Tanaka and Tachikawa, 2015; Sayama et al., 2020). For the comparison in terms of quick runoff response during storm event, the saturated hydraulic conductivity should be set higher than representative value. Therefore, we set the uniformly high saturated hydraulic conductivity and focus on the impact of different water retention parameters on the applicability of the proposed model. The relaxation time τ and the initial condition of S were determined from numerical experiments using the vertical one-dimensional Richards equation shown in Appendix A. For the initial condition in the 2D-RE, the average water content that the initial S is divided by the soil thickness was set to be uniform in the soil layer. In the 1D-New, we set $a = -\cos\phi$ as the initial condition. The Manning's roughness coefficient used in the surface flow model was set as $0.1 \text{ [m}^{-\frac{1}{3}} \bullet \text{ sec]}$. However, no cases with surface flow were observed in the simulations of this study due to the high saturated hydraulic conductivity. Therefore, we note that the Manning's roughness coefficient does not affect the results of this study.

Fig. 5 shows the rainfall input data. The rainfall data is the basin-averaged rainfall previously used in Sugawara and Sayama (2021). Event 1 is a single-peak event with a total rainfall of 239 mm, while event 2 shows a more complex temporal pattern with a total rainfall of 382 mm.

4. Results

4.1. Model comparison with several water retention curves

We compared the simulated runoff of the unit area from the slope and the storage-runoff relationship ($S-q$) at the slope outlet. In the 2D-RE, S and q were calculated by integrating the values of the grid cells

facing the outlet. To evaluate the performance of the proposed model, the Nash-Sutcliffe efficiency coefficient (NSE) for the 1D-New and 1D-Hs (NSE_{1D_New} and NSE_{1D_Hs}) is calculated assuming the runoff of the 2D-RE as true values. Fig. 6 shows hydrographs of event 1 with the parameter sets No. 1–4. In the No. 1 parameter representing loam, the 2D-RE shows the time-delayed and gentler runoff than the 1D-Hs. The 1D-New shows the storage effect that delays and reduces the peak runoff, similar to the 2D-RE ($NSE_{1D_New} = 0.99$ and $NSE_{1D_Hs} = 0.88$). In the No. 2 parameter representing sand, the 2D-RE stores more rainwater before the peak time than the 1D-New, but the peak runoff is larger in 2D-RE ($NSE_{1D_New} = 0.78$ and $NSE_{1D_Hs} = 0.59$). The difference is because the relaxation time τ , which is assumed to be constant, considerably varies even in the wet condition by the weak nonlinearity of the unsaturated hydraulic conductivity. Hence, the pressure head distribution tends to be nonlinear by drying the near soil surface according to the low water retention even when the saturated zone occurs. In the No.3 and No.4 parameters representing clay and silt, respectively, the runoff is small, with almost no difference among the three models. For clay and silt, the threshold value (i.e., $S_{thre}(-\cos\phi)$) at which the saturated zone on the bedrock may occur is high owing to their water retention properties, and the storage value in event 1 did not exceed this value. In this case, no saturated zone occurs for any pressure head distribution, and the lateral discharge becomes low for all models, regardless of the percolation process.

Fig. 7 shows storage-runoff relationships ($S-q$) of the event 1 with the parameter sets No. 1–4. The path represents changes over time, and the arrows indicate the direction of change. The time of the largest runoff corresponds to the peak time. In the 1D-Hs, the storage-runoff relationship is a one-to-one correspondence. However, in the 1D-New and 2D-RE, it shows hysteresis over time because the runoff is different even for the same S . For the No.1 loam parameter, the runoff of the 1D-New and the 2D-RE is suppressed because the rainwater that infiltrates into the soil layer does not immediately accumulate on the bedrock, unlike with the 1D-Hs, and is absorbed by the soil layer through the percolation process. For the same storage (S) condition, the

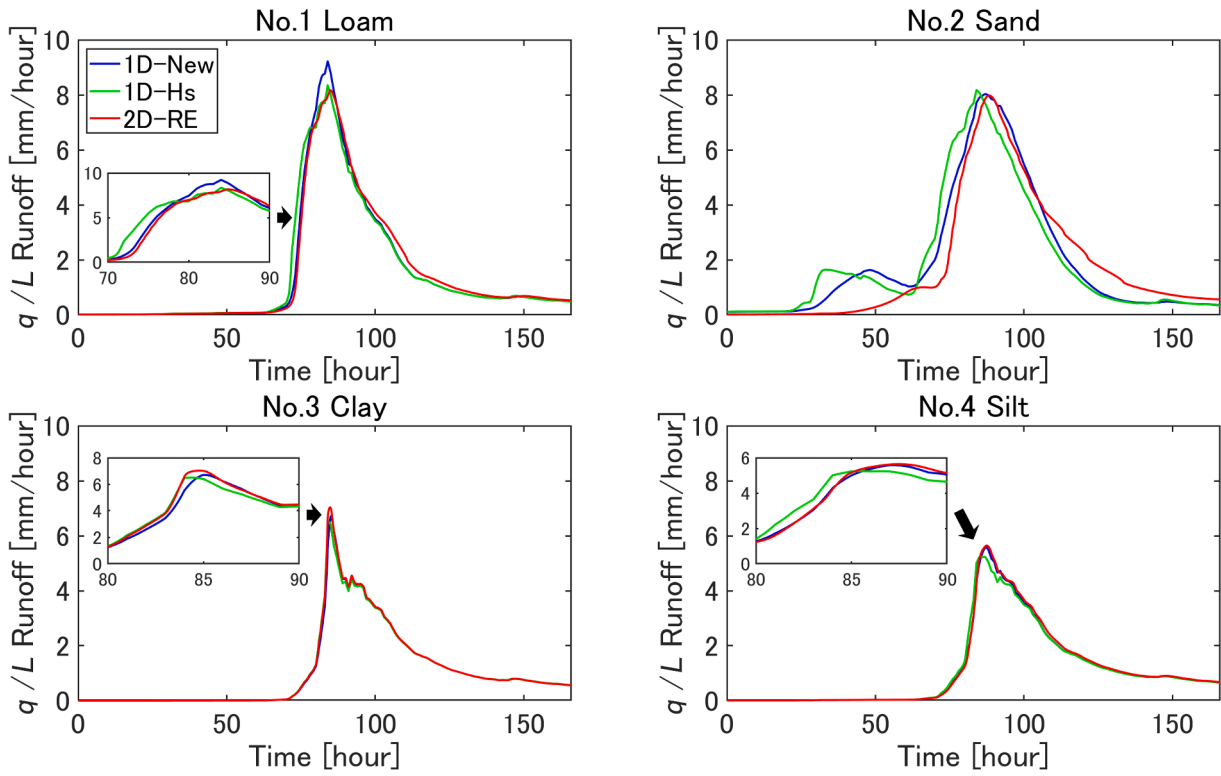


Fig. 8. Hydrographs of event 2 with the parameter sets No.1-4.

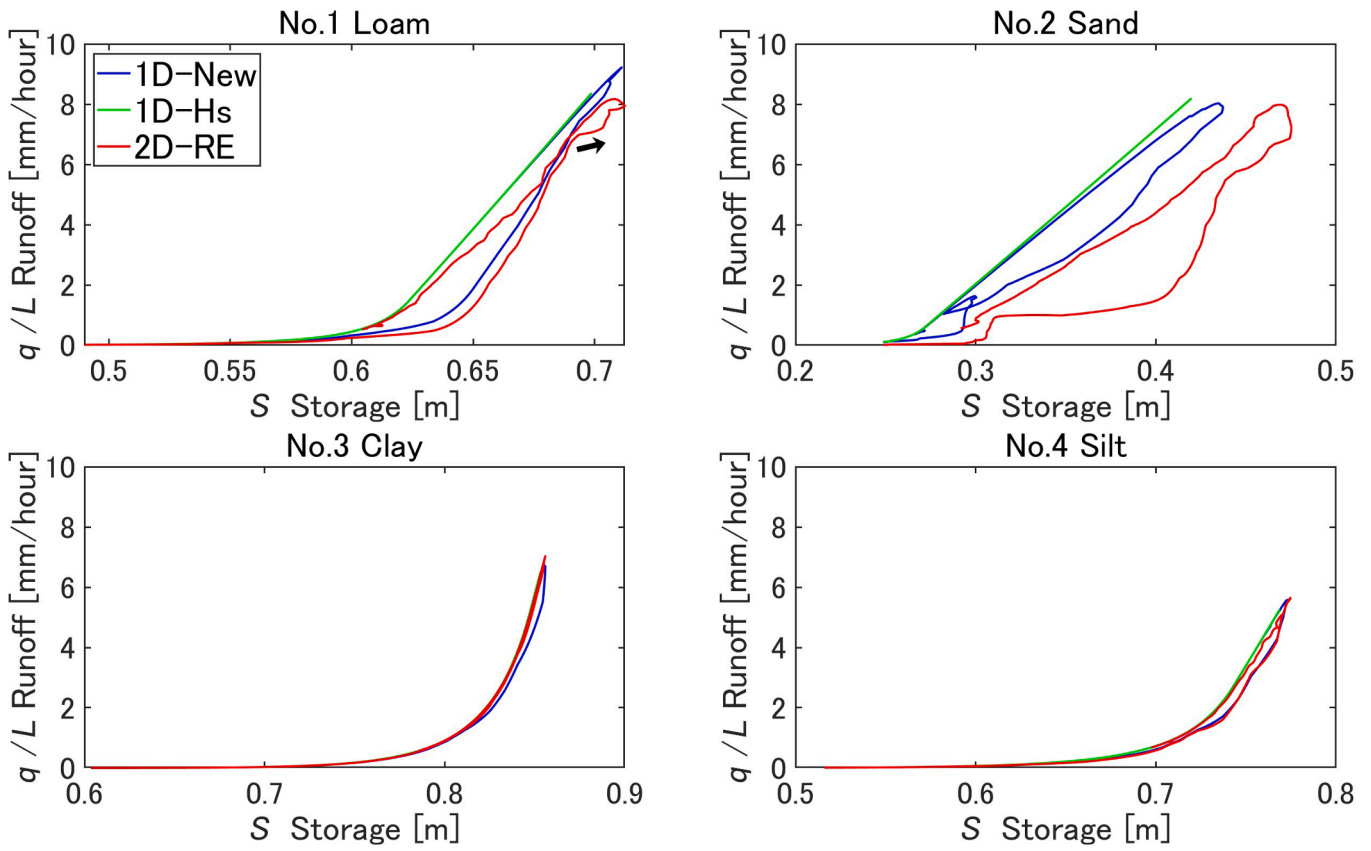


Fig. 9. Storage-runoff relationships of event 2 with the parameter sets No.1-4. The arrow indicates the effect that the unsaturated zone stores rainwater even in high S condition because the near soil surface become dry.

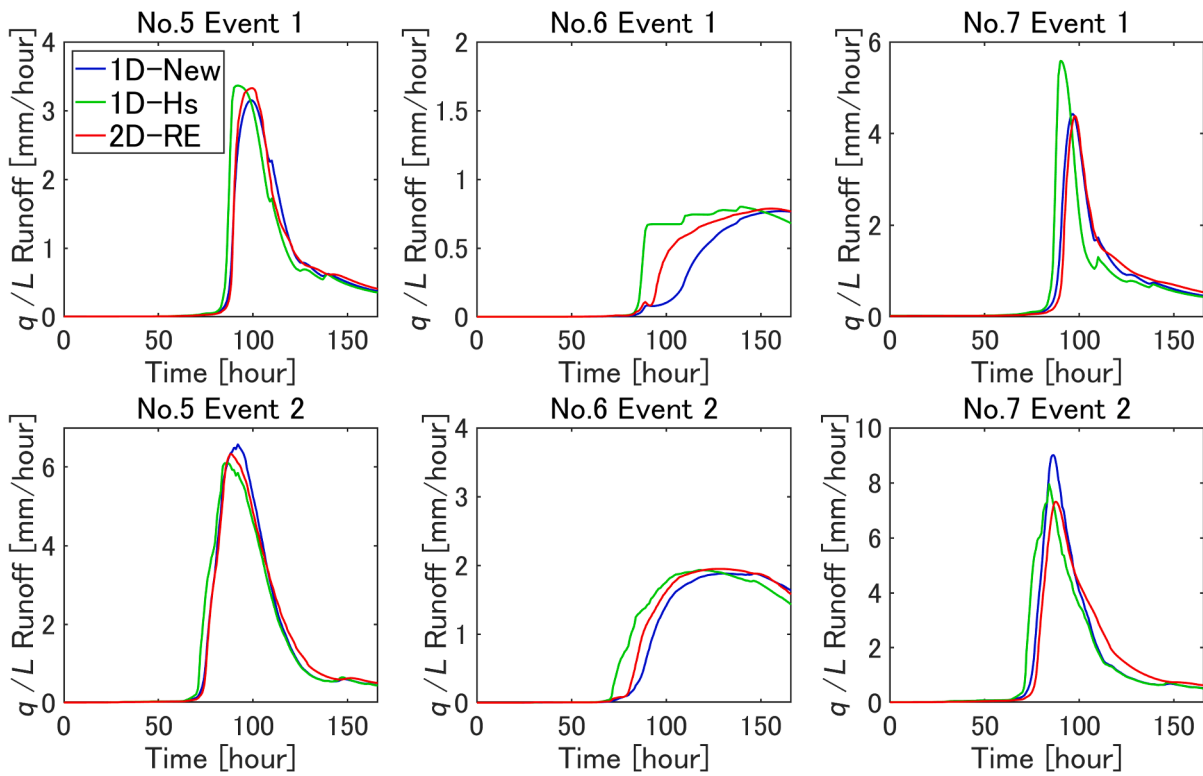


Fig. 10. Hydrographs of event 1 and 2 with the parameters sets No. 5-7.

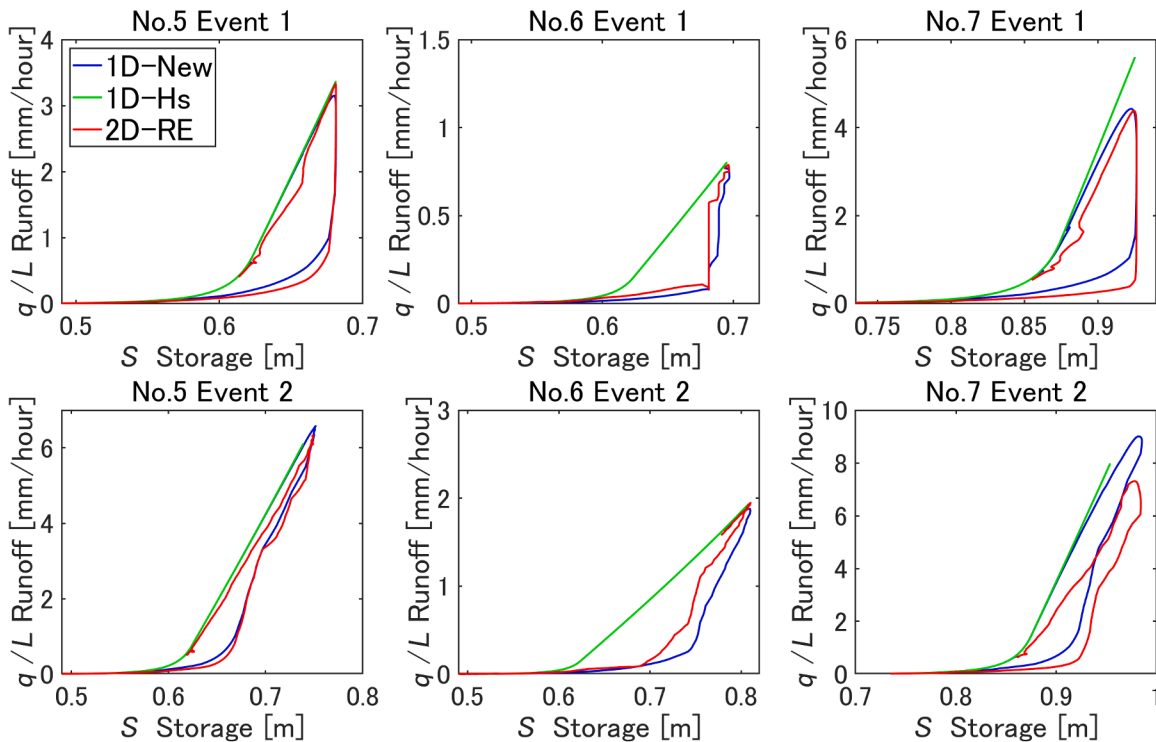


Fig. 11. Storage-runoff relationships of event 1 and 2 with the parameters sets No. 5-7.

runoff after the peak is higher than before the peak because of the pooling of rainwater on the impervious bedrock with completing percolation. For the No. 2 sand parameter, the 1D-New shows the hysteresis similar to the 2D-RE, but the 2D-RE has a larger loop. This is due to the storage before the peak time and the large peak runoff, as

described earlier in the explanation of the hydrograph. For the No. 3 clay and No. 4 silt parameters, the storage-runoff relationships had almost no difference among the three models.

Fig. 8 shows the hydrographs of event 2 with the parameter sets No.1-4. For the No.1 loam parameter, the difference between the 1D-Hs

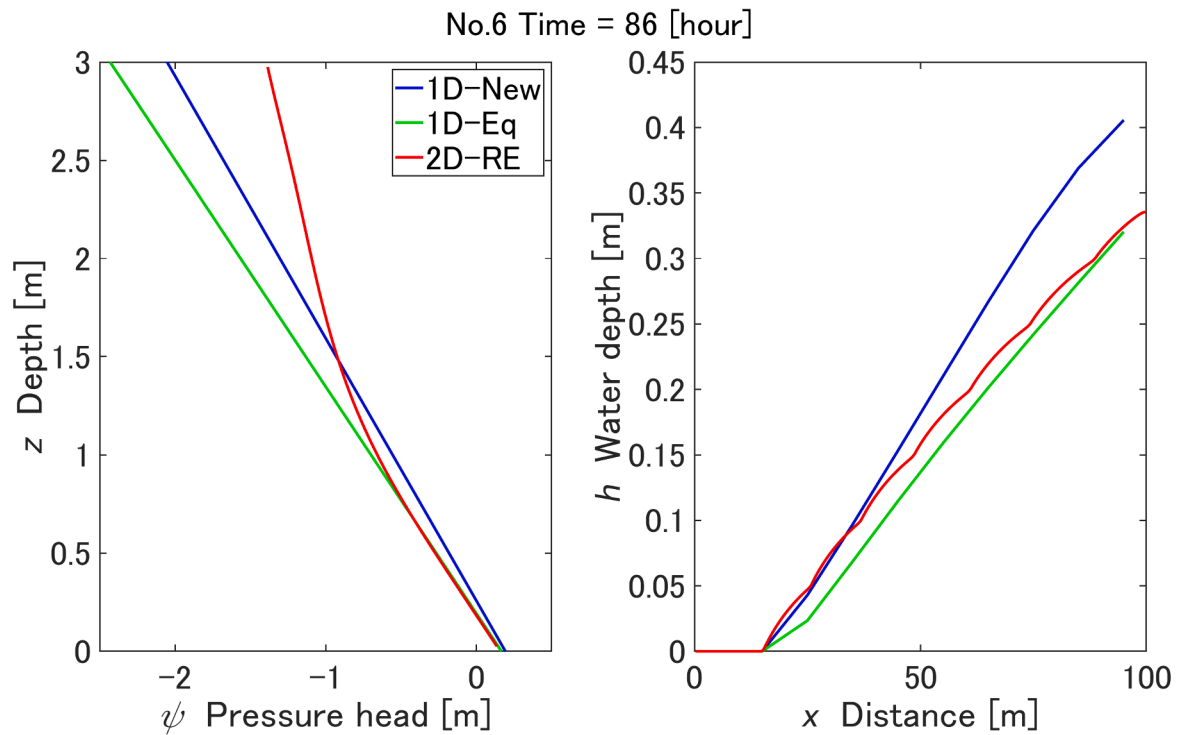


Fig. 12. (left) Pressure head distributions at the outlet cross-section at the 1D-New peak time in event 2 with the parameter set No. 7. (right) Water depth distributions at the 1D-New peak time in event 2 with the parameter set No. 7. x is the distance from the top of slope.

and 2D-RE is smaller than that in event 1 ($NSE_{1D-Hs} = 0.96$). This is because the soil layer becomes wetter owing to the increased total rainfall, and the effect of percolation becomes small. However, the storage effect of reducing the runoff before the peak time is still evident, but the 1D-New can reproduce it ($NSE_{1D-New} = 0.99$). For the No. 2 sand parameter, the 1D-New reproduces the peak runoff and time delay of the 2D-RE, although the storage before the peak time is lower than that in the 2D-RE ($NSE_{1D-New} = 0.90$ and $NSE_{1D-Hs} = 0.78$). For the No. 3 clay parameter, the runoff is larger than it is in event 1 because of the saturated zone caused by the increased total rainfall. Similar to event 1, almost no difference exists among the three models. However, the reason for this seems to differ from that for event 1. The clay parameter has a high water retention characteristic which keeps the entire soil layer wet and allows percolation to finish quickly. For the No. 4 silt parameter, the difference among the three models is still small owing to the high water retention characteristic of the silt, but the 1D-New and 2D-RE models show a slight storage effect.

Fig. 9 shows the storage-runoff relationships of event 2 with the parameter sets No.1–4. For the No.1 loam parameter, the 2D-RE shows the storage effect that suppresses the increase in the runoff as indicated by the arrow even in the wet condition. This is due to the drying near the soil surface by the progress of percolation, even in the wet condition, which occurs the saturated zone. In this case, the 1D-New, which assumes the linear pressure head distribution, does not reproduce the 2D-RE because both sides near the bedrock and soil surface become wet. For the No. 2 sand parameter, the 2D-RE similarly shows the storage effect because the near soil surface is easy to dry. However, for the No. 3 clay and No. 4 silt parameters, the storage effect, as indicated by the arrow in the result of the No. 1 loam parameter, is almost negligible. This is because the high water retention characteristics of the clay and silt keep the near soil surface moist without drying out.

In summary, the newly developed 1D-New reproduces accurately the behavior of the 2D-RE for clay and silt. For loam, the 1D-New also reproduces the behavior of the 2D-RE, but the pressure head becomes nonlinear when both sides near soil surface and the bedrock are wet, causing differences. For sand, the difference between the 1D-New and

2D-RE is larger than that of other soil types because the pressure head distribution tends to be nonlinear and the relaxation time τ significantly varies even in wet conditions.

4.2. Model comparison for the different saturated hydraulic conductivity and soil layer thickness

Fig. 10 and Fig. 11 show the hydrographs and storage-runoff relationships for events 1 and 2, illustrating the effects of cutting the saturated conductivity in half and into tenth (parameter sets No. 5 and 6) and increasing the soil depth from 2 m to 3 m (parameter set No.7). For the case of parameter set No. 5, a smaller hydraulic conductivity reduces the peak runoff and elongates the response time; the hydrograph is less abrupt. This is partly because percolation takes longer, resulting in more water being stored in the soil layer. The discrepancy between the 1D-Hs and 2D-RE exists for the lower permeability ($NSE_{1D-Hs} = 0.87$, 0.96 in events 1 and 2). However, the 1D-New with modified τ based on the saturated hydraulic conductivity accurately reproduces the behavior of the 2D-RE ($NSE_{1D-New} = 0.99$, 0.99 in events 1 and 2). In event 2, the ratio of the peak runoff of the 1D-New and 2D-RE is 1.13 for the parameter set No. 1 and 1.04 for the parameter set No. 5, showing a smaller difference with lower permeability. This is because the drainage reduction keeps the near soil surface wet, and the nonlinearity of pressure head distribution becomes weak. A similar trend was observed in the case of parameter set No. 6, which further reduces the saturated hydraulic conductivity. The 1D-New shows higher NSE values and better reproducibility than the 1D-Hs ($NSE_{1D-Hs} = 0.83$, 0.95 and $NSE_{1D-New} = 0.87$, 0.98 in events 1 and 2).

For the 1 m thicker soil layer represented in the parameter set No.7, the distance of unsaturated percolation became longer, and more rainwater was stored in the soil layer. As in the case of the parameter set No.5, the difference between the 1D-Hs and 2D-RE with the parameter set No. 7 was large ($NSE_{1D-Hs} = 0.17$ and 0.72 in events 1 and 2), and the 1D-New accurately reproduces the behavior of the 2D-RE in event 1 ($NSE_{1D-New} = 0.95$ and 0.91 in events 1 and 2). However, in event 2, the difference in peak runoff between the 1D-New and 2D-RE with the

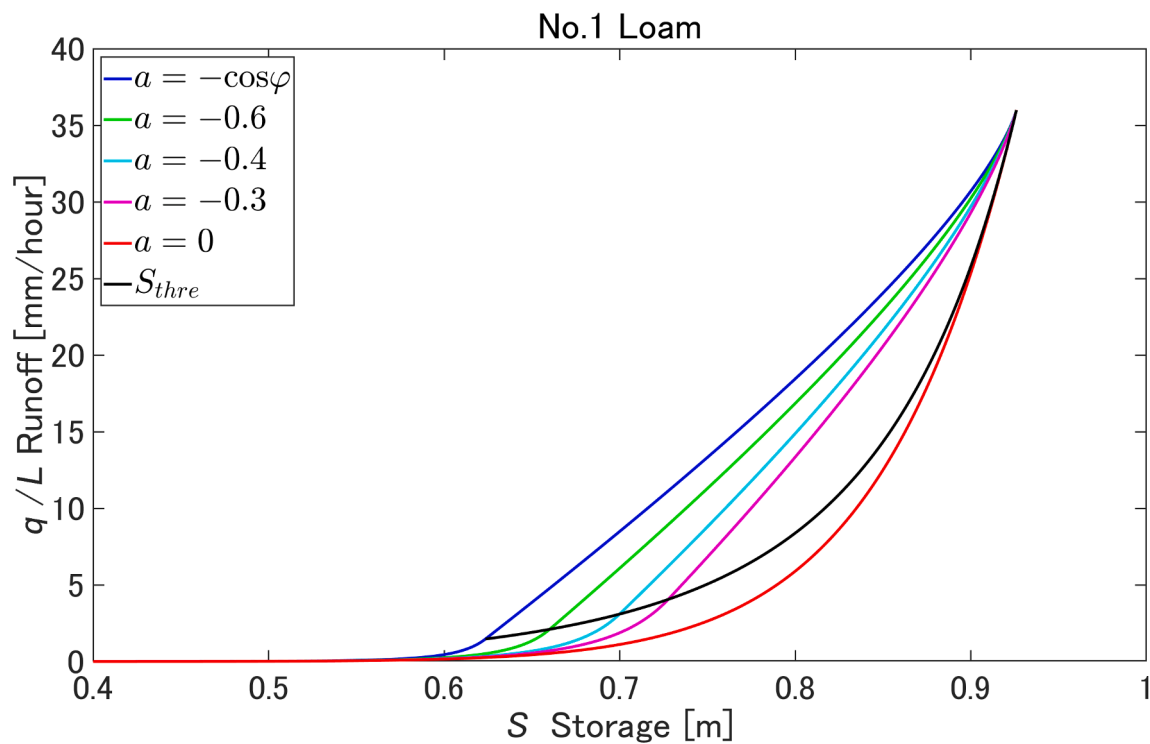


Fig. 13. Storage-runoff relationship of the 1D-NEW based on the several pressure head gradients a and the parameter set No.1. S_{thre} at which the saturated zone begins to occur is defined in equation (13).

parameter set No. 7 was greater (approximately 23 %). This is because the unsaturated zone was expanded, and the pressure head distribution of the 2D-RE became non-linear (Fig. 12). For shallower soils ($z > 2$ m), the pressure head of the 2D-RE was higher than that of the other two models, and the distribution is nonlinear. By contrast, the distribution of 1D-New indicate that the rainwater was more quickly transported to the lower area of the soil layer. Thus, the previous and new one-dimensional approach with the approximation of the pressure-depth relationship as linear overestimates the rate of re-wetting from the second pulse of rainfall. This occurs over the entire slope (Fig. 12). The 1D-Hs shows the smallest water depth because it is already draining at the peak of the 1D-New. The 2D-RE shows a smaller water depth than that of the 1D-New because of the storage effect in the unsaturated zone during the second rainfall pulse, which suppresses the development of the saturated zone.

In summary, for smaller saturated hydraulic conductivity, the soil layer stores more rainwater owing to slow percolation, and this suppressed drainage makes it easier to keep the entire soil layer wet. Consequently, the applicability of the 1D-New, which linearly approximates the pressure head, may be improved. In that case, the 1D-New accurately reproduces the behavior of the 2D-RE. Moreover, for the deeper soil layer thickness, the storage in the soil layer increases owing to the longer percolation distance. For the simple rainfall pattern such as event 1, the 1D-New and 2D-RE agree well. However, for more complex rainfall patterns such as event 2, the pressure head distribution of the 2D-RE shows nonlinearity, resulting in a large difference with the 1D-New.

5. Discussion

5.1. Characteristics of the proposed model

Section 4 demonstrated that the 1D-Hs cannot completely represent the 2D-RE. Similar results have been reported in previous studies comparing lateral flow models with the Richards equation (e.g., Broda

et al., 2012; Jeannot et al., 2018). One approach to the issue is to couple the lateral flow model with the one-dimensional vertical Richards equation (e.g., Pikul et al., 1974; Abbott et al., 1986; Downer and Ogden, 2004; Hilberts et al., 2007). As described in the introduction, this method has the advantage of solving percolation rigorously, but it requires three-dimensional discretization, which increases the computational cost. However, the 1D-New, the new KW model considering percolation, can reproduce the effect of making runoff gentle and delayed, as well as the Richards equation. In addition, the new model is superior to the lateral flow models coupled with the Richards equation in terms of computational cost since it does not require discretization along the perpendicular direction.

The main differences between the existing lateral flow models assuming the hydrostatic condition (Pan et al., 2015; Kong et al., 2016; Sugawara and Sayama, 2021) and our proposed model involves considering the vertical gradient of the pressure head in the new model. To evaluate the impact of the vertical gradient, we showed the storage-runoff relationship of the 1D-New based on the several pressure head gradients a and the parameter set No. 1. (Fig. 13). For the hydrostatic condition ($a = -\cos\phi$), the 1D-New is the same as the 1D-Hs and the runoff is the maximum for a unique S value. Runoff is minimized by imposing a homogeneous vertical pressure head distribution (i.e., $a = 0$). The runoff above the S_{thre} curve is the case when the saturated zone exists. In the 2D-RE, percolation causes the hysteretic loop of the storage-runoff relationship. The 1D-New can reproduce this behavior of the 2D-RE by considering the different distributions for a unique S value. However, the previous lateral flow models assuming the hydrostatic condition show single distribution for each S value, and cannot reproduce the hysteresis, which is an important characteristic of hillslope storage-runoff relationships (Penna et al., 2011). Some models describe percolation without spatial discretization (e.g., Qu and Duffy, 2007; Jeong and Park, 2017; Muñoz-Carpena et al., 2018). Those models are mainly constructed by separating percolation in the unsaturated zone from saturated lateral flow. Such an approach is clear because it isolates each hydrological process, but the interaction between processes (e.g.,

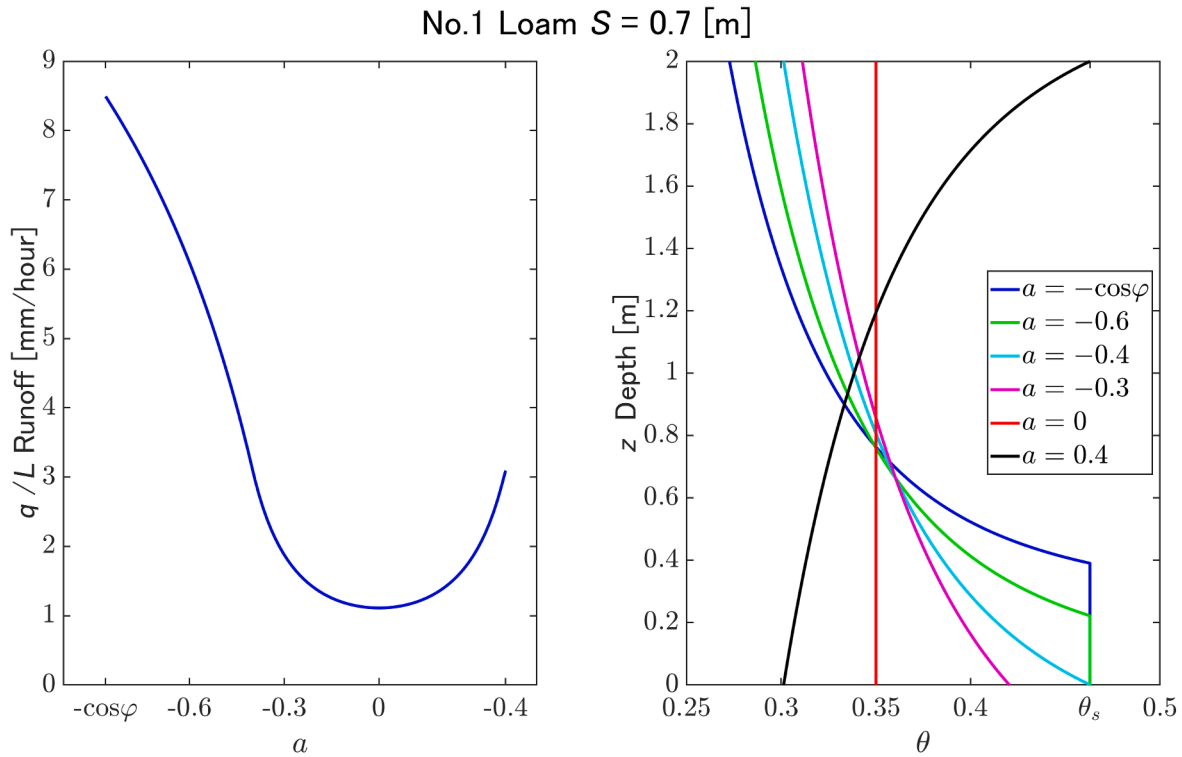


Fig. 14. (left) Relationship between runoff and a based on the parameter set No. 1 when $S = 0.7$ [m]. (right) Distributions of water content θ along the z direction.

changes in percolation distance as the water table rises) often become complicated. The uniqueness of the proposed method is that the water storage in the unsaturated and saturated zones can be tracked in a single continuity equation. This allows for seamless handling of percolation and lateral flow. The relationship of water distributions and runoff in the proposed method is shown in Fig. 14. The runoff is maximum at the hydrostatic condition ($a = -\cos\varphi$), and is minimum for the homogeneous distribution ($a = 0$). If a increases in $-\cos\varphi \leq a \leq 0$, the runoff monotonically decreases. This is because of the decrease in the wet zone at the bottom of the soil layer. If a increases in $0 < a \leq 0.4$, the wet area at the soil surface inversely expands and the runoff monotonically increases. In the proposed method, the storage ratio between the unsaturated and saturated zones is expressed as variable a . Furthermore, we can integrate percolation and lateral flow by deriving the analytical relationship between total water storage and runoff.

The percolation effect in the 1D-New model changes depending on the parameter τ . We analyzed the impact of the parameter τ on runoff in Appendix B.

5.2. Robustness of the parameter τ for initial condition and estimation method of τ from soil property

In the proposed model 1D-NEW, we assume the linear pressure head distribution and percolation expressed by the change of the pressure head gradient a . This allows the effect of percolation to be easily reflected in the lateral subsurface model. The change in a by progress of percolation depends on the newly introduced parameter τ . Therefore, investigating the robustness of the parameter τ for initial condition and discussing how to estimate τ from soil property are important. In this section, we discuss these two points.

To investigate the robustness of the parameter τ for different initial conditions, we simulated for all cases with the new initial conditions which varied ± 0.4 [m] from the initial conditions shown in Table 2. Fig. 15 shows the hydrographs around the peak time. We calculated the difference in NSE as follows.

$$\Delta NSE = NSE_{new_initial} - NSE_{default} \quad (31)$$

$NSE_{new_initial}$ is NSE calculated with the new initial condition and $NSE_{default}$ calculated with the initial condition shown in Table 2. We calculated ΔNSE in 28 cases (7 parameter sets \times 2 events \times 2 initial conditions). For ΔNSE in all cases, the mean was -0.0033 and the median was 0.0011 . The maximum ΔNSE was 0.072 (the parameter set No. 6, event 1, and initial condition $+0.4$ [m]) and the minimum ΔNSE was -0.079 (the parameter set No. 2, event 2, and initial condition -0.4 [m]). From this result, we confirmed that τ used in this study is the robust parameter for different initial conditions. The robustness of τ can be explained as follows. The effect of percolation in hillslope runoff appears as the hysteresis in the storage-runoff relationship. For all simulations with parameter sets presented in this study, the hysteresis was greater in wet than in dry conditions. This is because the differential of the relative hydraulic conductivity is greater the closer to saturation, and the sensitivity of the lateral discharge q to the pressure head distribution is greater in wet conditions, where high water content area can be formed, than in dry conditions, where high water content area cannot be formed. Therefore, from the perspective of runoff during storm event, to select τ which can reproduce changes in the pressure head gradient a in wet conditions is important. However, the differential of τ to soil moisture is larger in dry conditions and smaller in wet conditions (see Appendix A). Therefore, the range of τ to be selected is in wet conditions and its range is narrow, and the single value of τ may be applicable to different initial conditions.

Percolation is strongly influenced by three components: the saturated hydraulic conductivity, water retention curve, and soil layer thickness. Therefore, we consider estimating τ from these parameters. We assume that τ is inversely proportional to the saturated hydraulic conductivity because Darcy velocity is proportional to the saturated hydraulic conductivity regardless of volumetric water content and the numerical experiments in Appendix A showed an inversely proportional relationship between τ and the saturated hydraulic conductivity. In order to express the soil layer thickness and water retention curve in a

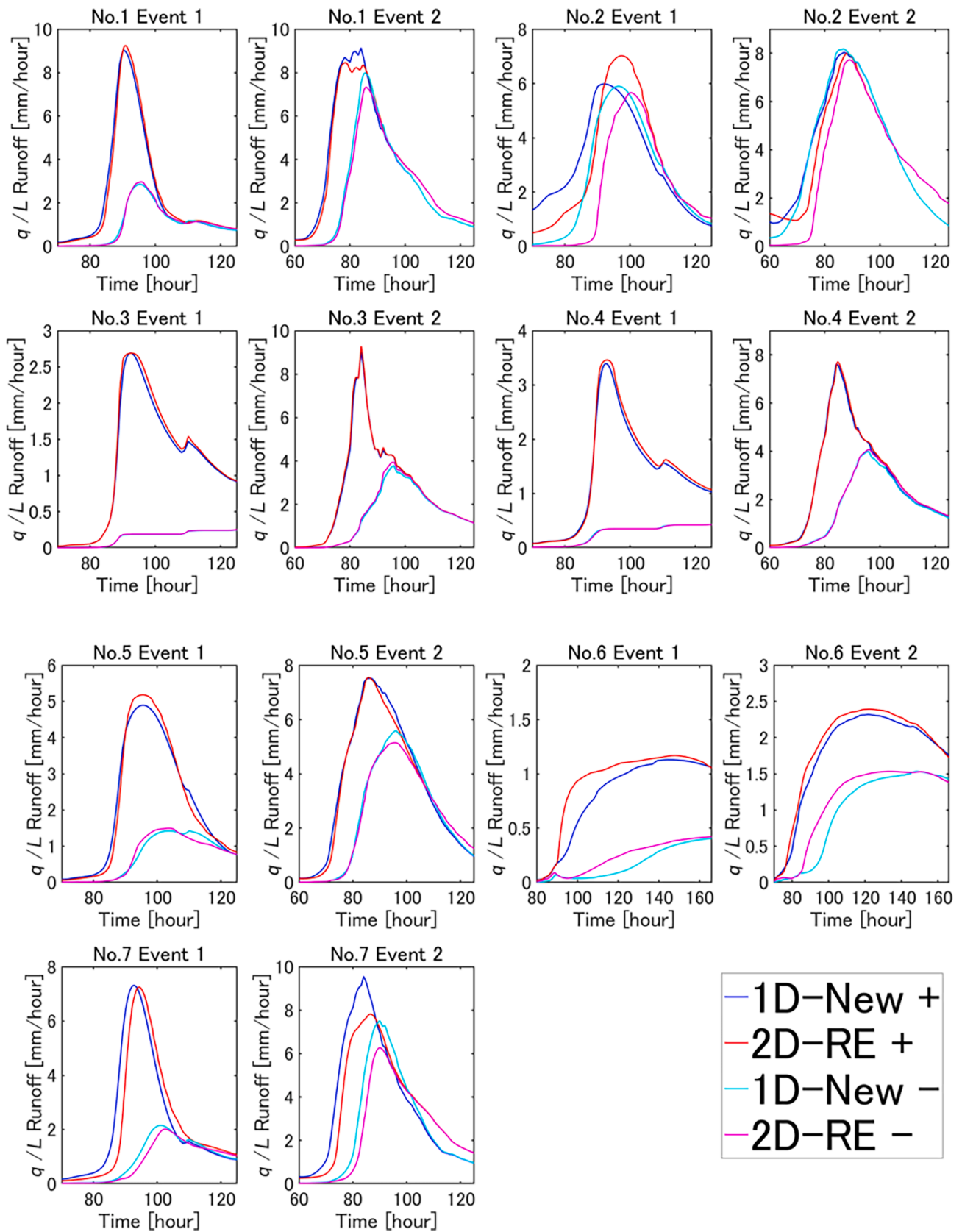


Fig. 15. Hydrographs around the peak time for all cases with new initial conditions which varied ± 0.4 [m] from the initial conditions shown in Table 2. The symbol + indicates $+0.4$ [m] initial condition and the symbol - indicates -0.4 [m] initial condition.

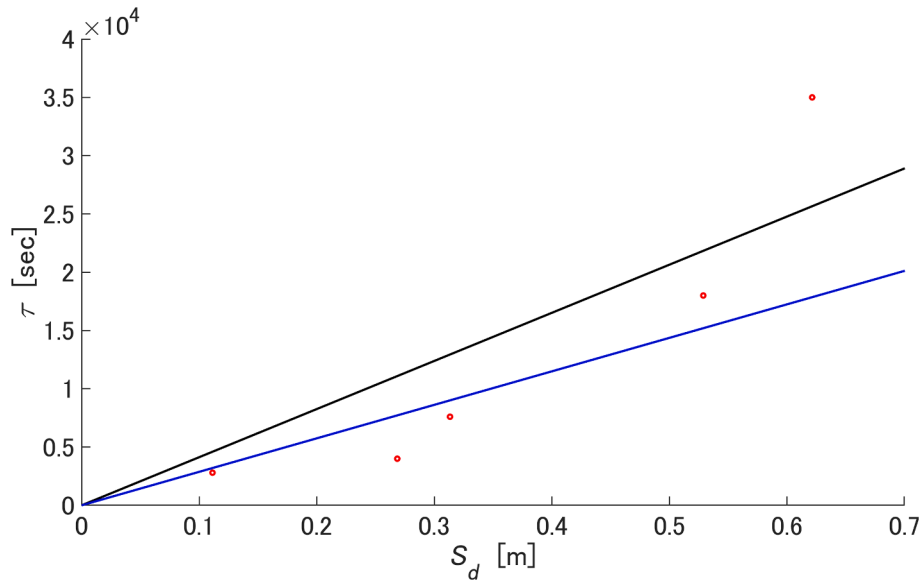


Fig. 16. Relationship between S_d and τ for the parameter sets with $k_s = 0.001$ [m/sec] in Table 2. The black line represents the linear regression for all data and the blue line represents the linear regression for data excluding sand with low NSE. (For interpretation of the references to colour in this figure legend, the reader is referred to the web version of this article.)

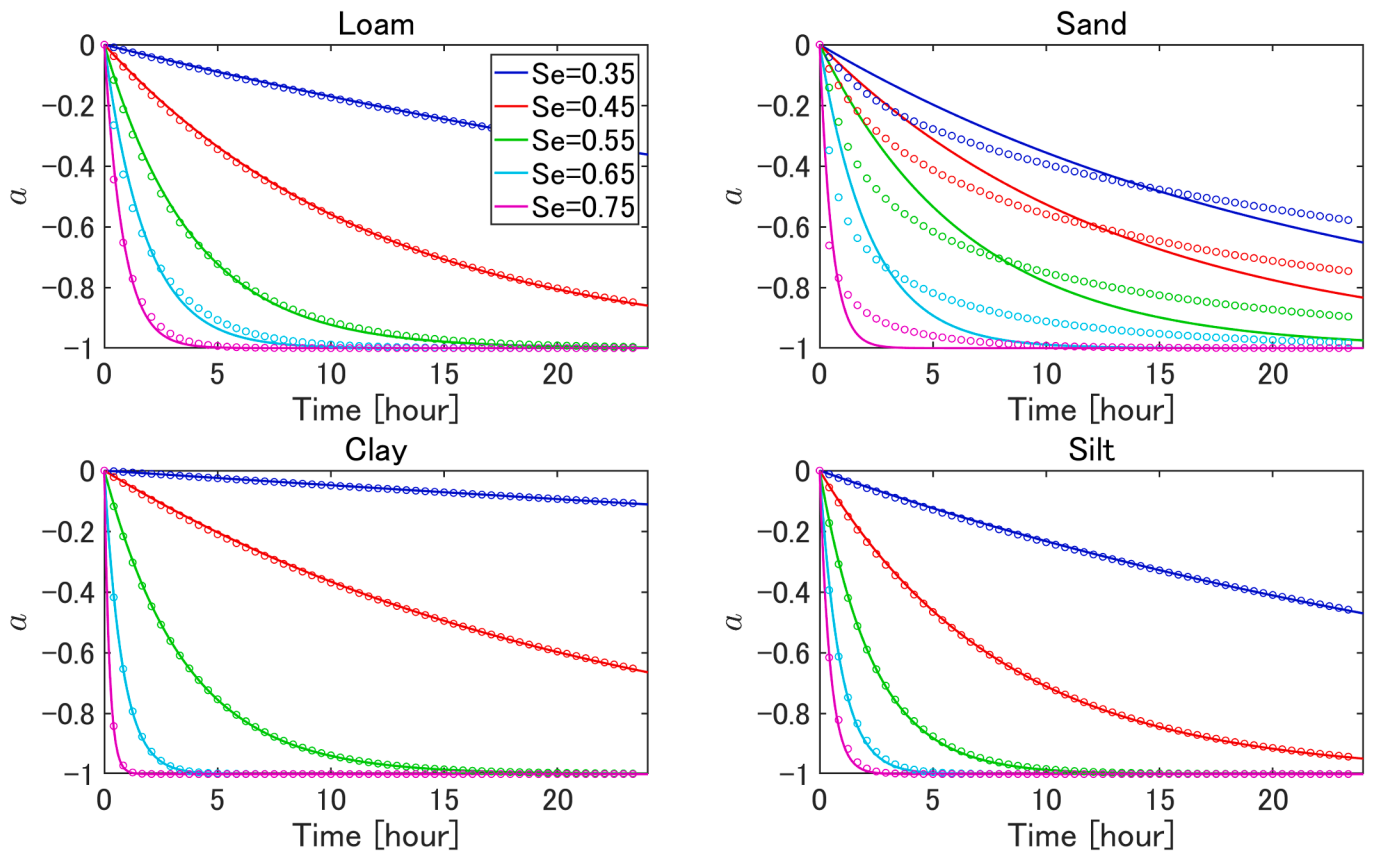


Fig. A1. Time variation of the pressure head gradient a calculated from numerical experiments of the one-dimensional Richards equation (the circle) and the exponential decay model with optimized τ (the solid line).

single index, we introduce the storage deficit S_d [L]:

$$S_d = \theta_s D - S_{thre}(a = -1) = (\theta_s - \theta_r) D + \frac{\psi_e(\theta_s - \theta_r)}{(1 - \lambda)} \left[1 - \left(\frac{\psi_e - D}{\psi_e} \right)^{1-\lambda} \right] \quad (32)$$

$S_{thre}(a = -1)$ is the storage volume at which $\psi_b = \psi_e$ under the hydrostatic condition when we consider the soil column with the parameters of interest. That is to say, S_d represents how much rainwater can be stored once the storage S reaches the value at which the saturated zone can be formed. The larger S_d , the larger τ , since the storage effect ap-

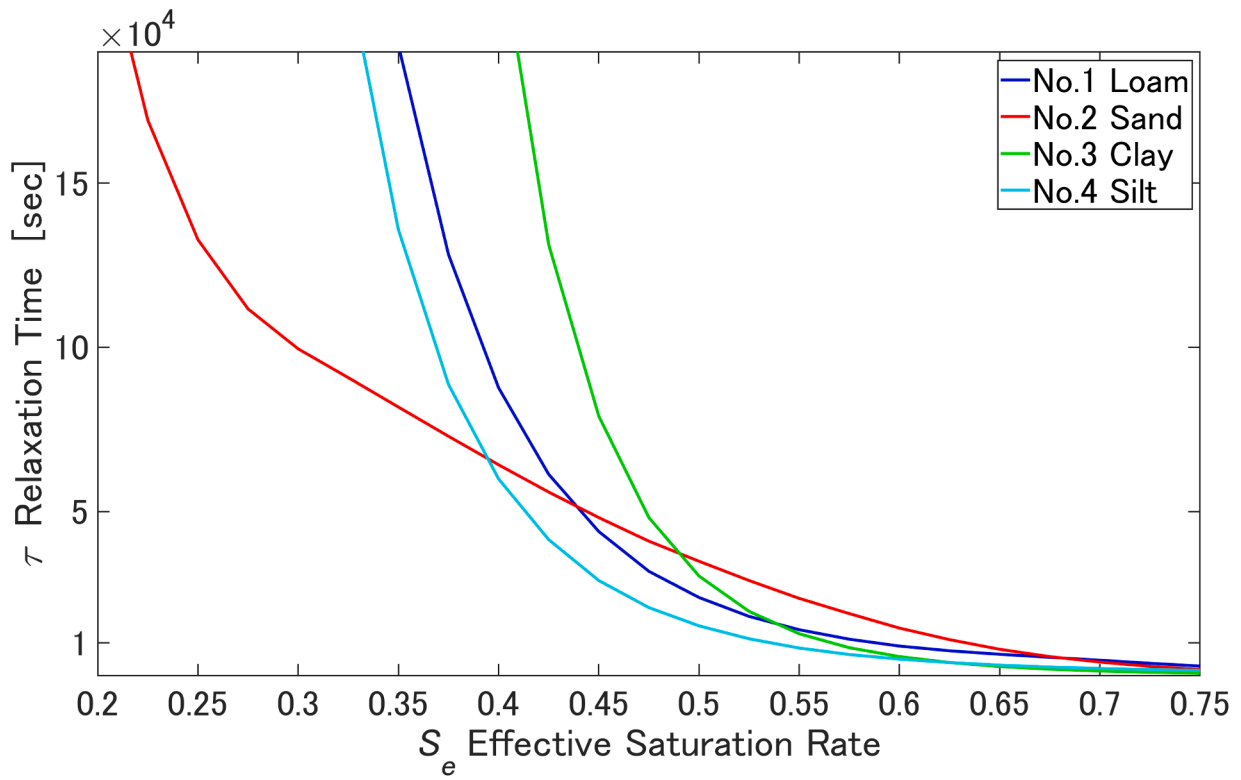


Fig. A2. Variations of τ for initial S_e with the parameter sets No. 1–4.

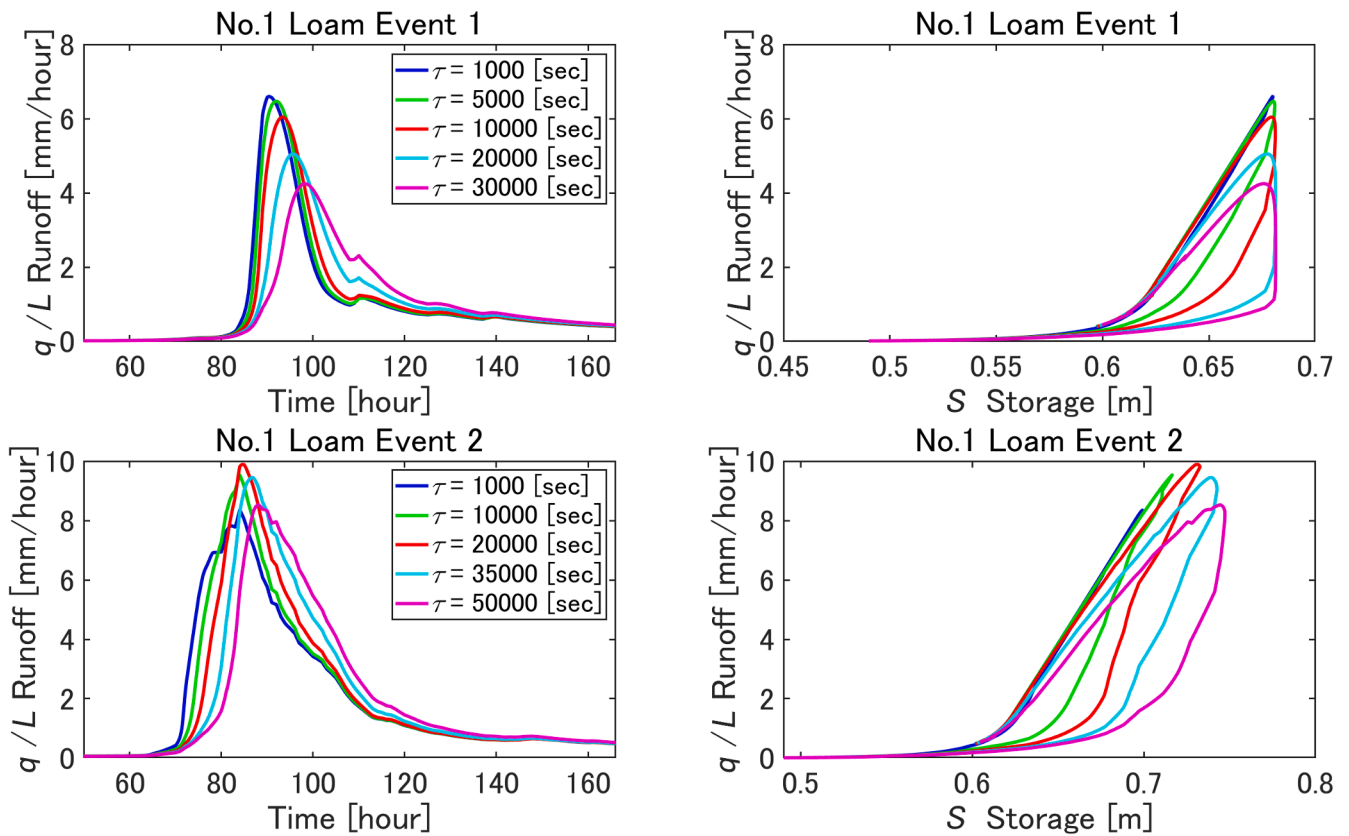


Fig. B1. Hydrographs and storage-runoff relationships of event 1 and 2 with the parameter set No. 1, but τ is changed to several values.

pears even in wet conditions. Fig. 16 shows the relationship between S_d and τ for the parameter sets with $k_s = 0.001$ [m/sec] in Table 2. It should be noted that the number of data in this study is small, but the results suggest that τ increases as S_d increases. More data should be obtained from simulations by using the proposed model and the numerical solutions of the Richards equation for various soil properties and optimizing τ to the results of the Richards equation. If we assume a linear relationship between S_d and τ , the estimated equation for τ is as follows.

$$\tau = 0.001\alpha \frac{S_d}{k_s} \quad (33)$$

where α is the proportionality coefficient between S_d and τ , and the coefficient 0.001 indicates that α is regressed on data with $k_s = 0.001$ [m/sec]. $\alpha = 42000$ for all data (the black line in Fig. 16), and $\alpha = 29000$ for data excluding sand with low *NSE* (the blue line in Fig. 16). A similar expression of characteristic time is used to define the time to reach the field capacity (Assouline and Or, 2014). If τ in this study could be related to an index such as the field capacity, estimating τ could be easier.

6. Conclusions

In this study, we improved the KW model, which simulates the lateral flow in steep hillslopes, to consider the effect of percolation along the direction perpendicular to the bedrock. Specifically, the perpendicular distributions of the pressure head, which had been assumed to be the hydrostatic condition, were extended to the non-hydrostatic condition. By assuming that the pressure head distributions are linear, we derived the relationships between the storage and runoff that do not require perpendicular discretization. This allows the KW model to reproduce the effect of percolation with low computational cost.

To analyze the response of the newly developed model (1D-New), we compared the 1D-New, the KW model assuming the perpendicular hydrostatic condition (1D-Hs), and the numerical solution of the two-dimensional Richards equation (2D-RE). Focusing on the water retention characteristics, the 1D-New almost reproduces the behavior of the 2D-RE when the water retention characteristics are strong. For weak water retention characteristics, the difference between the 1D-New and 2D-RE is more likely to occur because of the low applicability of two assumptions as the linearity of pressure head and constant relaxation time τ . When the saturated hydraulic conductivity is lower, the difference between the 1D-Hs and 2D-RE is clear regarding the peak runoff and time delay, but the 1D-New can reproduce the response of the 2D-RE. When the soil layer thickness is deeper, the 1D-New can repro-

duce the behavior of the 2D-RE in events with the simple rainfall waveform. However, as the rainfall waveform is complex, the pressure head distribution becomes nonlinear, and the difference between the 1D-New and the 2D-RE increases.

The newly developed KW model can reproduce the storage effect seen in the Richard equation. However, the applicability of the assumptions used for the derivation seems to be lower when the water retention characteristics are weak or when the soil layer thickness is deep. The ultimate goal of the study is to reproduce the rainfall-runoff processes in real watersheds using a hydrological model. Applying the developed model to a distributed runoff model and discussing its applicability by comparison with observed data is necessary in future studies.

CRediT authorship contribution statement

Yoshito Sugawara: Conceptualization, Methodology, Software, Validation, Writing – original draft. **Takahiro Sayama:** Conceptualization, Writing - Review & Editing, Funding acquisition.

Declaration of competing interest

The authors declare that they have no known competing financial interests or personal relationships that could have appeared to influence the work reported in this paper.

Data availability

Data will be made available on request.

Acknowledgements

We thank to Prof. Yutaka Ichikawa of Kyoto University for the valuable discussion. We also thank to Assoc. Prof. Hyunuk An of Chungnam National University for sharing the source code to solve the Richards equation. We appreciate the helpful comments from Prof. John Selker of Oregon State University. This work was supported by MEXT-Program for The Advanced Studies of Climate Change Projection (SENTAN) [grant number JPMXD0722678534]; Council for Science, Technology and Innovation (CSTI), Crossministerial Strategic Innovation Promotion Program (SIP), “Enhancement of Societal Resiliency against Natural Disasters” (PI: Prof. Hori) and “Development of a Resilient Smart Network System against Natural Disasters” (Funding agency: NIED); and JSPS KAKENHI [grant number 19H02248] (PI: Sayama).

Appendix A: Estimation of the parameter τ

To estimate the values of the relaxation time τ , the new parameter added to the KW model developed in this study, we conducted simulations using a numerical solution of the vertical one-dimensional Richards equation. The numerical solution was constructed by changing the settings of the 2D-RE. The one-dimensional vertical Richards equation is

$$\frac{\partial \theta}{\partial t} = \frac{\partial}{\partial z'} K \left(\frac{\partial \psi}{\partial z'} + 1 \right) \quad (A1)$$

where z' is the vertical upward coordinate. The spatial resolution is $\Delta z' = 0.05$ [m], and the iterative calculation method is similar to that of the 2D-RE. The no flow boundary condition was used for the upper and lower boundary conditions. The initial conditions were set as various values of the effective saturation rate S_e uniformly throughout the soil column. We used the parameters shown in Table 2.

The time variation of the pressure head gradient a was calculated by linearly approximating the vertical distribution of the pressure head at each time step. In addition, we optimized τ by comparing these results with the equation for calculating a in the 1D-New. For the above simulation settings, we need to modify equation (23) as $\cos \phi = 1$, $a^{temp} = 0$, $a^{ij} = a$ and $\Delta t = t$. The equation becomes

$$a = \exp\left(-\frac{t}{\tau}\right) - 1 \quad (A2)$$

We obtained the optimized τ for each initial condition by selecting τ with which the root mean squared error between the simulation results and equation (A.2) is the smallest. Fig. A.1 shows the time variation of the pressure head gradient a calculated from numerical experiments of the one-dimensional Richards equation and the exponential decay model with optimized τ . For loam, clay, and silt, the exponential decay model is able to reproduce the change in a calculated from the one-dimensional Richards equation. For sand, the exponential decay model may be less applicable due to the low accuracy of the linear approximation of the pressure head distribution in the first place. The percolation process in hillslope is much more complex than this numerical experiment. However, the purpose of this study is not to solve percolation process rigorously, but rather to provide a simplified representation of percolation process and then reflect its effects in the lateral subsurface model. Therefore, we believe it is reasonable to adopt the exponential decay model that can reproduce the change in a calculated from the one-dimensional Richards equation. In addition, since the proposed model focuses on the runoff response during storm event, it is important for the change in a to reproduce the response during wet conditions, such as when saturated zones are occurring. Therefore, it is important to use the fitted τ for wet conditions in the rainfall-runoff translation during a storm event, and we think that the effect of the change in τ with soil moisture is relatively small. Also, under conditions where saturated zones occur, $a \leq 0$, which is also consistent with the setting of this experiment.

Fig. A.2 shows the variations of τ for the initial S_e with the parameter sets No. 1-4. Naturally, when the initial S_e is larger, it takes a shorter time to reach hydrostatic because the soil column is wet. In the results of No.1 loam, No.3 clay and No.4 silt, τ was sensitive to the initial S_e in $S_e \leq 0.5$. This is because of a strong nonlinearity of the unsaturated hydraulic conductivity in an extremely dry condition. If we adopt the values of τ in this range, we may underestimate the runoff in hillslopes. However, in $S_e \geq 0.75$, τ was very small and insensitive to the initial S_e because the soil column was extremely wet. Therefore, if we adopt the values of τ in this range, we cannot consider the percolation effect, and the 1D-New is almost consistent with the 1D-Hs. From these results, we assume that the values of τ in $0.5 < S_e < 0.75$ are suitable for the parameters to be used in the 1D-New, and their average values were adopted. In addition, the initial conditions to be used in the comparative simulations of the 1D-New, 1D-Hs and, 2D-RE are set to the storage S converted from the values $S_e = 0.5$ – 0.55 , which are conditions in which water is adequately drained. We used the same idea for the No. 2 sand. However, the range of τ , which is not extremely dry or wet, is wider than that of other soil types because of the weak nonlinearity of the unsaturated hydraulic conductivity. The applicability of the assumption that τ is constant seems to be less than that for other soil types.

From the simulation with No. 5, 6 and 7, the value of τ with No. 5, 6 and 7 was approximately 2, 10, and 2.4 times greater, respectively, than it was with No. 1. The estimation method in this appendix is a qualitative procedure; therefore, an optimization using observation data or regarding τ as a function of S may improve the accuracy of the developed model.

Appendix B: Effects of the parameter τ on the runoff

The 1D-New can simulate various water content distributions by varying a and, thereby, reproduce the percolation effect, leading to more gradual runoff and delayed flow. The temporal dynamics of a are determined by the relaxation time τ (equation (24)). Therefore, it is important to investigate the effects of the time-scale parameter τ on the runoff and storage. A larger τ increase the time to reach the hydrostatic condition (slower percolation).

In the hydrograph of event 1, increasing τ from 0.25 h to 8.3 h delayed the runoff by about 8 h and reduced the peak by up to 35 % (Fig. B.1) is because slower percolation suppresses the development of the saturated zone, and more rainwater is stored in the unsaturated zone. Since rainwater stored in the unsaturated zone flows slower, the base flow becomes larger. In the storage-runoff relationship of event 1, a larger τ results in the wider storage-runoff hysteretic loop, requiring more water to initiate runoff. The loop of the storage-runoff relationship becomes sharper for a smaller τ , and it is almost non-existent when $\tau = 1000$ [sec]. Therefore, as expected, when τ is small, the 1D-New shows almost the same response as the 1D-Hs. Showing more complex behavior, in event 2, an intermediate τ slightly delays the rise of the hydrograph and also increases peak outflow by approximately 20 % (Fig. B1). In $\tau = 1000$ – $20,000$ [sec], the peak runoff increases with τ . This may be because of the more temporal variation in the rainfall of event 2. The first peak is delayed and combined with the second one to form a large peak. In $\tau = 20,000$ – $50,000$ [sec], the peak runoff becomes smaller for the larger τ owing to increased storage in the unsaturated zone (as seen in event 1). Considering the storage-runoff relationship of event 2, for the larger τ , the hysteresis is more gradual, also consistent with that seen for event 1. However, the storage S at the time of the peak runoff clearly changes with τ unlike those in event 1 because of the longer rainfall period of event 2.

Appendix C. Supplementary data

Supplementary data to this article can be found online at <https://doi.org/10.1016/j.jhydrol.2024.130726>.

References

- Abbott, M.B., Bathurst, J.C., Cunge, J.A., O'connell, P.E., Rasmussen, J., 1986. An introduction to the european hydrological system—Systeme Hydrologique European, "SHE", 2: structure of a physically-based, distributed modelling system. *J. Hydrol.* 87 (1–2), 61–77. [https://doi.org/10.1016/0022-1694\(86\)90115-0](https://doi.org/10.1016/0022-1694(86)90115-0).
- Alfieri, L., Thielen, J., Pappenberger, F., 2012. Ensemble hydro-meteorological simulation for flash flood early detection in southern Switzerland. *J. Hydrol.* 424, 143–153. <https://doi.org/10.1016/j.jhydrol.2011.12.038>.
- An, H., Ichikawa, Y., Yorozu, K., Tachikawa, Y., Shiiba, M., 2010. Validity assessment of integrated kinematic wave equations for hillslope rainfall-runoff modeling. *Ann. J. Hydraulic Eng. (JSCE)* 54, 505–510.
- An, H., Yu, S., 2014. Finite volume integrated surface-subsurface flow modeling on nonorthogonal grids. *Water Resour. Res.* 50 (3), 2312–2328. <https://doi.org/10.1002/2013WR013828>.
- Arnold, J.G., Srinivasan, R., Muttliah, R.S., Williams, J.R., 1998. Large area hydrologic modeling and assessment part I: model development 1. *JAWRA J. Am. Water Resour. Assoc.* 34 (1), 73–89. <https://doi.org/10.1111/j.1752-1688.1998.tb05961.x>.
- Assouline, S., Or, D., 2014. The concept of field capacity revisited: Defining intrinsic static and dynamic criteria for soil internal drainage dynamics. *Water Resour. Res.* 50 (6), 4787–4802. <https://doi.org/10.1002/2014WR015475>.
- Beven, K., 1981. Kinematic subsurface stormflow. *Water Resour. Res.* 17 (5), 1419–1424. <https://doi.org/10.1029/WR017i005p01419>.
- Broda, S., Larocque, M., Paniconi, C., Haitjema, H., 2012. A low-dimensional hillslope-based catchment model for layered groundwater flow. *Hydrol. Process.* 26 (18), 2814–2826. <https://doi.org/10.1002/hyp.8319>.
- Brooks, R.H., Corey, A.T., 1966. Properties of porous media affecting fluid flow. *J. Irrig. Drain. Div.* 92 (2), 61–88. <https://doi.org/10.1061/JRCEA4.0000425>.
- Childs, E.C., 1971. Drainage of groundwater resting on a sloping bed. *Water Resour. Res.* 7 (5), 1256–1263. <https://doi.org/10.1029/WR007i005p01256>.
- Ciarapica, L., Todini, E., 2002. TOPKAPI: A model for the representation of the rainfall-runoff process at different scales. *Hydrol. Process.* 16 (2), 207–229. <https://doi.org/10.1002/hyp.342>.
- Downer, C.W., Ogden, F.L., 2004. GSSHA: Model to simulate diverse stream flow producing processes. *J. Hydrol. Eng.* 9 (3), 161–174. [https://doi.org/10.1061/\(ASCE\)1084-0699\(2004\)9:3\(161\)](https://doi.org/10.1061/(ASCE)1084-0699(2004)9:3(161)).
- Du, J., Xie, S., Xu, Y., Xu, C.Y., Singh, V.P., 2007. Development and testing of a simple physically-based distributed rainfall-runoff model for storm runoff simulation in humid forested basins. *J. Hydrol.* 336 (3–4), 334–346. <https://doi.org/10.1016/j.jhydrol.2007.01.015>.
- Dunne, T., Black, R.D., 1970. Partial area contributions to storm runoff in a small New England watershed. *Water Resour. Res.* 6 (5), 1296–1311. <https://doi.org/10.1029/WR006i005p01296>.

- Fan, Y., Bras, R.L., 1998. Analytical solutions to hillslope subsurface storm flow and saturation overland flow. *Water Resour. Res.* 34 (4), 921–927. <https://doi.org/10.1029/97WR03516>.
- Freeze, R.A., 1972. Role of subsurface flow in generating surface runoff: 2. Upstream Source Areas. *Water Resour. Res.* 8 (5), 1272–1283. <https://doi.org/10.1029/WR008i005p01272>.
- Hilberts, A.G., Troch, P.A., Paniconi, C., 2005. Storage-dependent drainable porosity for complex hillslopes. *Water Resour. Res.* 41 (6) <https://doi.org/10.1029/2004WR003725>.
- Hilberts, A.G., Troch, P.A., Paniconi, C., Boll, J., 2007. Low-dimensional modeling of hillslope subsurface flow: Relationship between rainfall, recharge, and unsaturated storage dynamics. *Water Resour. Res.* 43 (3) <https://doi.org/10.1029/2006WR004964>.
- Hunukumbura, P.B., Tachikawa, Y., Shiiba, M., 2012. Distributed hydrological model transferability across basins with different hydro-climatic characteristics. *Hydrol. Process.* 26 (6), 793–808. <https://doi.org/10.1002/hyp.8294>.
- Ichikawa, Y., An, H., Tachikawa, Y., 2021. A methodology to examine a depth-discharge constitutive equation for rainfall-runoff modelling. *Hydrol. Res. Lett.* 15 (2), 44–49. <https://doi.org/10.3178/hr.15.44>.
- Jeannot, B., Weill, S., Eschbach, D., Schmitt, L., Delay, F., 2018. A low-dimensional integrated subsurface hydrological model coupled with 2-D overland flow: Application to a restored fluvial hydrosystem (Upper Rhine River–France). *J. Hydrol.* 563, 495–509. <https://doi.org/10.1016/j.jhydrol.2018.06.028>.
- Jeong, J., Park, E., 2017. A shallow water table fluctuation model in response to precipitation with consideration of unsaturated gravitational flow. *Water Resour. Res.* 53 (4), 3505–3512. <https://doi.org/10.1002/2016WR020177>.
- Kampf, S.K., Burges, S.J., 2007. A framework for classifying and comparing distributed hillslope and catchment hydrologic models. *Water Resour. Res.* 43 (5) <https://doi.org/10.1029/2006WR005370>.
- Kollet, S.J., Maxwell, R.M., 2006. Integrated surface–groundwater flow modeling: A free-surface overland flow boundary condition in a parallel groundwater flow model. *Adv. Water Resour.* 29 (7), 945–958. <https://doi.org/10.1016/j.advwatres.2005.08.006>.
- Kong, J., Shen, C., Luo, Z., Hua, G., Zhao, H., 2016. Improvement of the hillslope-storage Boussinesq model by considering lateral flow in the unsaturated zone. *Water Resour. Res.* 52 (4), 2965–2984. <https://doi.org/10.1002/2015WR018054>.
- Kubota, J., Sivapalan, M., 1995. Towards a catchment-scale model of subsurface runoff generation based on synthesis of small-scale process-based modelling and field studies. *Hydrol. Process.* 9 (5–6), 541–554. <https://doi.org/10.1002/hyp.3360090506>.
- Mualem, Y., 1976. A new model for predicting the hydraulic conductivity of unsaturated porous media. *Water Resour. Res.* 12 (3), 513–522. <https://doi.org/10.1029/WR012i003p00513>.
- Muñoz-Carpena, R., Lauvernet, C., Carlier, N., 2018. Shallow water table effects on water, sediment, and pesticide transport in vegetative filter strips—Part 1: nonuniform infiltration and soil water redistribution. *Hydrol. Earth Syst. Sci.* 22 (1), 53–70. <https://doi.org/10.5194/hess-22-53-2018>.
- Pan, Y., Weill, S., Ackerer, P., Delay, F., 2015. A coupled stream flow and depth-integrated subsurface flow model for catchment hydrology. *J. Hydrol.* 530, 66–78. <https://doi.org/10.1016/j.jhydrol.2015.09.044>.
- Paniconi, C., Marrocu, M., Putti, M., Verbunt, M., 2003. Newtonian nudging for a Richards equation-based distributed hydrological model. *Adv. Water Resour.* 26 (2), 161–178. [https://doi.org/10.1016/S0309-1708\(02\)00099-4](https://doi.org/10.1016/S0309-1708(02)00099-4).
- Penna, D., Tromp-van Meerveld, H.J., Gobbi, A., Borga, M., Dalla Fontana, G., 2011. The influence of soil moisture on threshold runoff generation processes in an alpine headwater catchment. *Hydrol. Earth Syst. Sci.* 15 (3), 689–702. <https://doi.org/10.5194/hess-15-689-2011>.
- Pikul, M.F., Street, R.L., Remson, I., 1974. A numerical model based on coupled one-dimensional Richards and Boussinesq equations. *Water Resour. Res.* 10 (2), 295–302. <https://doi.org/10.1029/WR010i002p00295>.
- Qu, Y., Duffy, C.J., 2007. A semidiscrete finite volume formulation for multiprocess watershed simulation. *Water Resour. Res.* 43, W08419. <https://doi.org/10.1029/2006WR005752>.
- Rawls, W. J., Brakensiek, D. L., Saxton, K. E., 1982. Estimation of soil water properties. *Trans. Am. Soc. Agric. Eng.*, 25(5), 1316–1320. 10.13031/2013.33720.
- Ross, P.J., Smettem, K.R.J., 2000. A simple treatment of physical nonequilibrium water flow in soils. *Soil Sci. Soc. Am. J.* 64 (6), 1926–1930. <https://doi.org/10.2136/sssaj2000.6461926x>.
- Sayama, T., McDonnell, J.J., 2009. A new time-space accounting scheme to predict stream water residence time and hydrograph source components at the watershed scale. *Water Resour. Res.* 45 (7) <https://doi.org/10.1029/2008WR007549>.
- Sayama, T., Ozawa, G., Kawakami, T., Nabesaka, S., Fukami, K., 2012. Rainfall–runoff–inundation analysis of the 2010 Pakistan flood in the Kabul River basin. *Hydrol. Sci. J.* 57 (2), 298–312. <https://doi.org/10.1080/02626667.2011.644245>.
- Sayama, T., Yamada, M., Sugawara, Y., Yamazaki, D., 2020. Ensemble flash flood predictions using a high-resolution nationwide distributed rainfall-runoff model: case study of the heavy rain event of July 2018 and Typhoon Hagibis in 2019. *Prog. Earth Planet Sci.* 7 (1), 1–18. <https://doi.org/10.1186/s40645-020-00391-7>.
- Sugawara, Y., and Sayama, T. (2021). Development of a storage discharge relationship to reflect water retention curve, and its application to a distributed runoff model. *J. Japan Soc. Civil Eng., Ser. B1 (Hydraulic Engineering)*, 77(1), 124–135. (In Japanese with English abstract) 10.2208/jscejhe.77.1_124.
- Tachikawa, Y., Nagatani, G., and Takara, K. (2004). Development of stage-discharge relationship equation incorporating saturated-unsaturated flow mechanism. *Annual J. Hydraulic Eng. (JSCE)*, 48, 7-12. (In Japanese with English abstract) 10.2208/prohe.48.7.
- Takasao, T., Shiiba, M., 1988. Incorporation of the effect of concentration of flow into the kinematic wave equations and its applications to runoff system lumping. *J. Hydrol.* 102 (1–4), 301–322. [https://doi.org/10.1016/0022-1694\(88\)90104-7](https://doi.org/10.1016/0022-1694(88)90104-7).
- Tanaka, T., Tachikawa, Y., 2015. Testing the applicability of a kinematic wave-based distributed hydrological model in two climatically contrasting catchments. *Hydrol. Sci. J.* 60 (7–8), 1361–1373. <https://doi.org/10.1080/02626667.2014.967693>.
- Tani, M., Matsushi, Y., Sayama, T., Sidle, R.C., Kojima, N., 2020. Characterization of vertical unsaturated flow reveals why storm runoff responses can be simulated by simple runoff-storage relationship models. *J. Hydrol.* 588, 124982 <https://doi.org/10.1016/j.jhydrol.2020.124982>.
- Thielen, J., Bartholmes, J., Ramos, M.H., De Roo, A., 2009. The European flood alert system—part 1: concept and development. *Hydrol. Earth Syst. Sci.* 13 (2), 125–140. <https://doi.org/10.5194/hess-13-125-2009>.
- Troch, P.A., Paniconi, C., Emiel van Loon, A.E., 2003. Hillslope-storage Boussinesq model for subsurface flow and variable source areas along complex hillslopes: 1. Formulation and characteristic response. *Water Resour. Res.* 39 (11) <https://doi.org/10.1029/2002WR001728>.